Applications of coupled cluster theory: from small hydrocarbons to potential circumstellar compounds

by

Walter Earl Turner II

(Under the direction of Henry F. Schaefer III)

Abstract

Ethylene is an exceptional example of a stable closed-shell singlet molecule with a low-lying triplet state of very different symmetry. The $\tilde{a}\ ^3A_1$ state of ethylene, which has a twisted D_{2d} geometry, is studied herein with coupled cluster theory. Geometric parameters are reported for C_2H_4, C_2D_4, and $^{13}C_2H_4$. Harmonic and anharmonic vibrational frequencies are also predicted using second-order vibrational perturbation theory. Challenges encountered for the wagging vibrational features are discussed.

Coupled cluster theory is further utilized to study the bonding, energetics, and vibrational frequecies of the the potential circumstellar molecule OPN. Isomers of OPN and several of its heavier group 15 and 16 congeners (SPN, SePN, TePN, OPP, OPAs, and OPSb) were examined. For OPN, OPP, and SPN, anharmonic vibrational frequencies and vibrationally corrected rotational constants are predicted; good agreement with available experimental data is observed.

Index words: Computational Chemistry, Theoretical Chemistry, Coupled Cluster, Triplet Ethylene, Anharmonic Frequencies, Spectroscopy, VPT2, Astrochemistry, Phosphorus Chemistry, Natural Resonance Theory, VY Canis Majoris

Applications of coupled cluster theory: from small hydrocarbons to potential circumstellar compounds

by

Walter Earl Turner II

B.S., Samford University, 2012

A Dissertation Submitted to the Graduate Faculty
of The University of Georgia in Partial Fulfillment
of the
Requirements for the Degree

Doctor of Philosophy

Athens, Georgia

2017

Applications of coupled cluster theory: from small hydrocarbons to potential circumstellar compounds

by

Walter Earl Turner II

Approved:

Major Professors: Henry F. Schaefer III

Committee: Gary E. Douberly
Gregory H. Robinson

Electronic Version Approved:

Dr. Suzanne Barbour
Dean of the Graduate School
The University of Georgia
May 2017

Acknowledgments

I first want to thank my parents, Walter and Othenia Turner, for supporting my academic endeavors, providing for me, and raising me to be a good person. I also thank my sister, Tanika, for her steadfast concern, encouragement, and empathy. My dear friends Soshawn, Jenee, Jordaan, Austin, and Ashley have been like an extended family and have always been there to laugh, cry, and celebrate with me.

I am grateful for Prof. Schaefer and his guidance and understanding. He has always supported me in my pursuits both in an out of chemistry. During the latter half of my first semester, I had to miss a research group meeting because of a choir concert and was terrified to tell Prof. Schaefer. He simply smiled and said, "Walter, we brought you here because of who you are and not in spite of it." Prof. Schaefer's commitment to high quality scientific research is truly awe inspiring. I aim to create a research group like his with an environment centered on respect, mentorship, and dedication to the science.

I have been blessed to have had wonderful chemistry teachers during my undergraduate and graduate studies. Dr. Wesley Allen and Dr. Paul Schleyer were instrumental in my development as a chemist. They both taught excellent classes and provided helpful discussions about my research and presentation skills. I will forever be indebted to my first chemistry professors Dr. Brian Gregory and Dr. David Garza for convincing me to change my major from Pre-Pharmacy to Chemistry. I would also like to thank my undergradate mentor Dr. Denise Gregory for providing me with my first undergraduate research opportunity. I will always appreciate her willingness to take a chance on a rising sophomore. Furthermore, I

would like to thank Dr. Morgan Ponder for introducing me to computational chemistry and arranging my participation in the CCQC summer research program.

It would be remiss of me if I did not thank the members of the Schaefer research group for their fruitful discussion and friendship, especially Kevin Moore, Avery Wiens, Bryan Soto, Sarah Elliot, Meghan Anand, Xiao Wang, Chenyang Li, Jonathon Vandezande, and Andreas Copan. Additionally, Dr. Justin Turney and Dr. Agarwal have provided invaluable guidance in my research. I would also like to thank the administrative staff members Sybil Zimmerman and Kathryn Juras for their friendship and help with paperwork.

Lastly, I would like to thank my UGA choir professors Dr. Daniel Bara and Dr. Gregory Broughton for the music we made together. Performances and rehearsals with your ensembles are some of my fondest graduate school memories.

Table of Contents

Chapter 1

Introduction and Literature Review

1.1 Introduction to Quantum Chemistry

Computational chemistry seeks to understand the structures, properties, and reactivities of molecules by solving the Schrödinger equation.[1] The time-independent, non-relativistic Schrödinger equation

$$\hat{H}|\Psi\rangle = E|\Psi\rangle \tag{1.1}$$

has been utilized by several chemists over the years. Equation 1.1 is an eigenvalue equation where The Hamiltonian operator, $\hat{H}$, is used to compute the energy, E, of the system.

$$\hat{H} = -\sum_{i=1}^{N}\frac{1}{2}\nabla_i^2 - \sum_{A=1}^{M}\frac{1}{2M_A}\nabla_A^2 - \sum_{i=1}^{N}\sum_{A=1}^{M}\frac{Z_A}{r_{iA}} + \sum_{i=1}^{N}\sum_{j>i}^{N}\frac{1}{r_{ij}} + \sum_{A=1}^{M}\sum_{B>A}^{M}\frac{Z_A Z_B}{R_{AB}} \tag{1.2}$$

The first two terms in equation 1.2 represent the kinetic energy of the electrons and nuclei, respectively. The last three terms account for the nuclear-electronic attraction, electron-electron repulsion, and nuclear-nuclear repulsion, respectively. The Hamiltonian operator acts on the wavefunction, Ψ, which is a probability amplitude that can be used to derive the probabilities for possible results of measurements made on the system. In equation 1.2, N is the number of electrons, M is the number of nuclei, and Z is the atomic number.

The position vectors r_{ij}, R_{AB}, and r_{iA} represent the electron-electron, nuclear-nuclear, and nuclear-electron distances, respectively.

As the electrons are much lighter than the nuclei, the electrons move significantly faster than do the nuclei. Chemists take advantage of this by employing the Born-Oppenheimer approximation, also called the "clamped nuclei" approximation. Under the Born-Oppenheimer approximation[2] the positions of the nuclei are "clamped" in place, and the electrons are treated as traveling in a static nuclear field. Accordingly, the term in equation 1.2 representing the nuclear kinetic energy may be neglected, and the term representing the nuclear-nucelar repulsion may be treated as a constant. The remaining terms are called the electronic Hamiltonian.

$$\hat{H}_{elec} = -\sum_{i=1}^{N} \frac{1}{2}\nabla_i^2 - \sum_{i=1}^{N}\sum_{A=1}^{M} \frac{Z_A}{r_{iA}} + \sum_{i=1}^{N}\sum_{j>i}^{N} \frac{1}{r_{ij}} \tag{1.3}$$

A constant accounting for the nuclear repulsion must then be added to the electronic Hamiltonian.

Owing to mathematical difficulties with computing the interelectron distances, r_{ij}, the electronic Hamiltonian is impossible to solve for anything other than the simplest systems.[3–7] Consequently, computational chemistry has become a field centered around systematically refining approximations in order to attain the best quantum chemical answers. Fortunately, even the simplest early approximations were quite sucessful when compared to known experimental results.[8–11]

In the pursuit of describing many electron systems, we can utilize functions describing the radial character of one electron in the component atom known as atomic orbitals.[12,13] These atomic orbtial functions may be linearly combined to define molecular orbitals.[14] In order to satisfy the antisymmetry requirement of the Pauli exclusion principle, antisymmetrized products of molecular orbitals are written as Slater determinants,

$$\Psi^{HF} = \frac{1}{\sqrt{N!}} \begin{vmatrix} \chi_a(\mathbf{x}_1) & \chi_b(\mathbf{x}_1) & \dots & \chi_N(\mathbf{x}_1) \\ \chi_a(\mathbf{x}_2) & \chi_b(\mathbf{x}_2) & \dots & \chi_N(\mathbf{x}_2) \\ \vdots & \vdots & \ddots & \vdots \\ \chi_a(\mathbf{x}_N) & \chi_b(\mathbf{x}_N) & \dots & \chi_N(\mathbf{x}_N) \end{vmatrix}. \tag{1.4}$$

The composite molecular orbtials describe both the spin and spatial distribution on one-electron, (χ_a). These Slater determinants are used to write the ground state wavefunction, resulting in the Hartree-Fock wave function. One can optimize the eigenvectors of the Hartree-Fock wave function using the self-consistent field method.[15] By then operating upon this improved wavefunction, one can obtain expectation values for the electronic energy as well as other observable physical quantities of the system at a specific geometry. Solution of the optimal set of molecular orbitals follows the variational principle,

$$\langle \Psi^{HF} | \hat{H} | \Psi^{HF} \rangle \leq \varepsilon_0, \tag{1.5}$$

where the expectation value of the Hamiltonian operating on the Hartree-Fock wavefunction is an upper bound to the exact electronic energy of the system.

However, the Hartree Fock approach is imperfect. By restricting the wavefunction to a single slater determinant, one implictly assumes that each electron only "feels" the average potential generated by all of the other electrons. Instead of this behavior, electrons actually "feel" each other instantly and avoid one other. These instantaneous interelectron interactions are described as the electron correlation effect. Thus, the difference in the Hartree-Fock energy and the true energy is called the correlation energy. By employing the Hartree-Fock approximation, one is able to recover 95 – 99% of the total energy for a given atomic or molecular system. While this is a substantial percentage of the total energy, several significant chemical phenomena such as electonic excitations, bonding, vibrational interactions, and molecular isomerization occur on the scale of this unaccounted energy. In

order to get relative energies within chemical accuracy, 1 kcal mol^{-1}, one must go beyond the Hartree-Fock approximation.

1.2 Coupled Cluster Theory

The method for recovering electron correlation primarily used in this dissertation is coupled cluster theory. It has been proven that if the coefficients of the entire set of Slater dermi-nants are ascertained, the time independent-relativistic electronic wave function would be exactly solved within the constraints of the chosen finite basis set. In coupled cluster theory, the products of substituted determinants are incorporated into the exponential "cluster" excitation operators, $e^{\hat{T}}$, in order to approximate the effects of higher order substitutions.

$$\Psi_{CC} = e^{\hat{T}}\Psi_{HF} \tag{1.6}$$

The form of the cluster operator is shown in equation 1.7

$$e^{\hat{T}} = 1 + \hat{T} + \frac{\hat{T}^2}{2!} + \frac{\hat{T}^3}{3!} + \dots. \tag{1.7}$$

where

$$\hat{T} = \hat{T}_1 + \hat{T}_2 + \hat{T}_3 \dots, \tag{1.8}$$

$$\hat{T}_1 = \sum_i \sum_a t_i^a a_a^\dagger a_i, \tag{1.9}$$

$$\hat{T}_2 = \frac{1}{4} \sum_{ij} \sum_{ab} t_{ij}^{ab} a_a^\dagger a_b^\dagger a_j a_i, \tag{1.10}$$

and in general

$$\hat{T_n} = \left(\frac{1}{n!}\right)^2 \sum_{ij\ldots}^{n} \sum_{ab\ldots}^{n} t_{ij\ldots}^{ab\ldots} a_a^\dagger a_b^\dagger \ldots a_i a_j. \tag{1.11}$$

We note that $\hat{T_n}$ is a n electron operator.

We will use the Hartree-Fock wavefunction, Ψ_{HF} as the reference wavefunction, Ψ_0. The coupled cluster wavefunction, $\Psi_{CC} \equiv \mathrm{e}^{\hat{T}}\ \Psi_0$, is used to approximate the exact wavefunction, Ψ. This changes the electronic Schrödinger equation (1.1) to

$$\hat{H} e^{\hat{T}} |\Psi_0\rangle = E e^{\hat{T}} |\Psi_0\rangle. \tag{1.12}$$

One can then utilize the projection technique to left multiply both sides of the equation by the reference Hartree-Fock wave function to obtain an expression for the energy

$$\langle \Psi_0 | \hat{H} e^{\hat{T}} | \Psi_0 \rangle = E \langle \Psi_0 | e^{\hat{T}} | \Psi_0 \rangle = E. \tag{1.13}$$

Here, we assume intermediate normalization, $\langle \Psi_0 | \Psi_{CC} \rangle = 1$. To further simplify the right hand side of equation 1.12, one can project it with e^{-T}

$$e^{-\hat{T}} \hat{H} e^{\hat{T}} |\Psi_0\rangle = E e^{-\hat{T}} e^{\hat{T}} |\Psi_0\rangle = E |\Psi_0\rangle. \tag{1.14}$$

In order to tackle the problem of the infinite expansion of $\hat{T}$,

$$\langle \Psi_0 | \hat{H} (1 + \hat{T} + \frac{\hat{T}^2}{2!} + \frac{\hat{T}^3}{3!} + \ldots) |\Psi_0\rangle = E \tag{1.15}$$

$$\langle \Psi_0 | \hat{H} | \Psi_0 \rangle + \langle \Psi_0 | \hat{H} \hat{T} | \Psi_0 \rangle + \langle \Psi_0 | \hat{H} \frac{\hat{T}^2}{2!} | \Psi_0 \rangle + \langle \Psi_0 | \hat{H} \frac{\hat{T}^3}{3!} | \Psi_0 \rangle + \cdots = E, \tag{1.16}$$

we may take advantage of Slater's rules. Since the Hamiltonian is at most a two electron

operator, and the cluster operator is at least a one electron operator, the terms $\hat{H}\hat{T^3}$ and higher cannot connect $\langle\Psi_0|$ and $|\Psi_0\rangle$. Therefore,

$$\langle\Psi_0|\hat{H}(1+\hat{T}+\frac{\hat{T}^2}{2!})|\Psi_0\rangle = E \tag{1.17}$$

for any level of truncation of $\hat{T}$.

One may obtain expressions for the cluster amplitudes by projecting the Schrodinger equation with the excited determinants produced by the action of the cluster operator on the reference,

$$\langle \Psi_{ij\ldots}^{ab\ldots} | \hat{H} e^{T} | \Psi_0 \rangle = E \langle \Psi_{ij\ldots}^{ab\ldots} | e^{\hat{T}} | \Psi_0 \rangle, \tag{1.18}$$

where $|\Psi_{ij\ldots}^{ab\ldots}\rangle$ represents an excited determinant in which orbitals ϕ_i, ϕ_j, etc. have been replaced with orbitals ϕ_a, ϕ_b, etc. Projections with the determinant $|\Psi_{ij}^{ab}\rangle$, for example, will produce an equation for the specific amplitude t_{ij}^{ab} (coupled to other amplitudes). By projecting equation 1.14 with the amplitudes, one may solve for the coupled cluster matrix elements.

$$\langle \Psi_i^a | e^{-T} H e^{T} | \Psi_0 \rangle = E \langle \Psi_i^a | \Psi_0 \rangle = 0 \tag{1.19}$$

$$\langle \Psi_{ij}^{ab} | e^{-T} H e^{T} | \Psi_0 \rangle = E \langle \Psi_{ij}^{ab} | \Psi_0 \rangle = 0 \tag{1.20}$$

1.3 Focal Point Analysis

While coupled cluster can greatly reduce the error of the Hartree-Fock method by recovering a significant portion of the correlation energy, the accuracy of the energy computations is still limited by the size of the basis set. Large flexible basis sets are needed to properly describe electron correlation but come with a greater computational expense. For the purpose of gaining the accuracy of larger basis sets without the associated computational expense, chemists have developed basis set extrapolation methods.

Chemists have published basis sets which systematically increase in size in a fashion which makes them extrapolatable to the infinite basis set limit. In this dissertation, I used the correlation consistent cc-pVXZ basis sets of Dunning. For these basis sets the Hartree-

Fock energies are extrapolated using the 3-point formula

$$E(X) = A + Be^{-CX}, \tag{1.21}$$

and the correlated energies are extrapolated using the 2-point formula

$$E(X) = A + BX^{-3}. \tag{1.22}$$

In the above equations X is the cardinality of the basis set, E is the energy, and A, B, and C are fitting parameters. Since we only extrapolate the occuppied orbitals acquired using Hartree-Fock theory, equation 1.21 approaches the CBS limit faster than equation 1.22. By computing the Hartree-Fock energy at three different cardinalities, one may use equation 1.21 to attain the values for A, B, and C. Similarly, by computing the correlated energy at two different cardinatilies, one may use equation 1.22 to attain the values for A and B. Once these value are attained, extrapolating the values for both the Hartree-Fock and correlated basis sets are straightforward

$$\lim_{X\to\infty} A + Be^{-CX} = A \tag{1.23}$$

$$\lim_{X\to\infty} A + BX^{-3} = A. \tag{1.24}$$

In this dissertation, we use the focal point technique for extrapolation. Previously, we noted the benefits of large basis sets. However, at some finite basis set size, there will be sufficient basis functions to describe the system, and increasing the basis set further will not change the energy. Additionally, one can observe that the energy difference between Hartree-Fock and second order Møller-Plessett perturbation theory (MP2) is much greater than the difference between MP2 and coupled clusted theory with single and double excitations

(CCSD).[16–18] Similarly, the difference between CCSD and CCSD(T)[19] is much smaller than either of these. That is to say, succesively higher excitations become systematically less important. Based on these two trends, the focal point approach[20–26] of Allen uses multiple computations to monitor the convergence of the system's energy to the complete basis set limit.

The focal point approach assumes that geometries determined at lower levels of theory are sufficiently accurate, and that the inaccuracy in relative energies is mainly due to insufficient treatment of electron correlation. Therefore, after computing the geometry at the highest feasible level of theory [e.g. CCSD(T)/cc-pVQZ], single-point energy computations are performed at several higher levels of theory with increasing basis set size. One can then use these computed single point energies to extrapolate to the complete basis set limit using equations 1.21 and 1.22. Here, we note that while the focal point technique does extrapolate the basis set to the infinite basis set limit, it does not extrapolate the electron correlation to the full configration interaction limit.

One may also assume that differences at high-level correlation are independent of basis set, e.g. CCSDT(Q) – CCSDT. This assumption is commonplace as corrections are relatively small to begin with. There is also a smaller probabilty of more than two electrons being close together. Furthermore, since triple excitations correlate three electrons simultaneously, quadruples correlate four, etc., and the wavefunction is zero at the coalescence point of more than two electrons, the wavefunction is zero.

A sample focal point table for the H_2 + CO $\rightarrow$ Formaldehyde reaction is shown in Table 1.1. As equations 1.21 and 1.22 only require 3 and 2 energies respectively in order to extrapolate to the full basis set limit, we notice that many of the numbers in the table do not contribute to the final answer, but serve as a diagnostic. What is more, the focal point table can always be extended if the convergence is not satisfactory. By including the lower

terms the error bars may be estimated. The focal point approach benefits from both its low computational cost and flexibility of execution.

1.4 Natural Resonance Theory

Resonance, Linus Pauling remarked,[27] "is now treated in essentially every textbook of chemistry and is used by essentially every chemist." Despite this widespread utilization, resonance theory primarily serves an instructional tool instead of a quantitative theory of chemical structure and reactivity.[28] The goal of Natural Resonance Theory is to present a practical numerical algorithm by which the results of contemporary *ab initio* calculations can be qualitatively expressed in the language of resonance theory.

Considering this, it is useful to add that a general molecular property, P, may be represented as

$$\langle P \rangle = \sum_{\alpha} \omega_{\alpha} \langle P \rangle_{\alpha}, \tag{1.25}$$

where ω_{α} are weighting factors such that

$$\begin{aligned} \omega_{\alpha} &\geq 0, \\ \sum_{\alpha} \omega_{\alpha} &= 1. \end{aligned} \tag{1.26}$$

Natural Resonance Theory[29] describes a resonance hybrid as an incoherent superposition of localized first-order density matrices.[30]

$$\hat{\Gamma} = \sum_{\alpha} \omega_{\alpha} \hat{\Gamma}_{\alpha} \tag{1.27}$$

Here, the true density operator, $\hat{\Gamma}$, is described as a weighted combination of a set of candidate density operators, $\hat{\Gamma}_{\alpha}$, for idealized localized resonance structures. A further premise is

that the stabilization energy provided by a resonance structure is proportional the weighting factor of that structure.

$$\Delta E_\alpha \propto \omega_\alpha \tag{1.28}$$

We can formulate this resonance-theoretic hypothesis (1.27) as a least-squares variation function of the unknown weighting factors, ω_α. The variational error of this resonance expansion can be measured by δ_ω

$$\delta_\omega = \min_{\{\omega_\alpha\}} \|\hat{\Gamma} - \sum_\alpha \omega_\alpha \hat{\Gamma}_\alpha\|. \tag{1.29}$$

The variational error, δ_ω will vanish if, and only if, 1.27 is an exact representation of the true density operator, $\hat{\Gamma}$. Likewise, For a single term expansion,

$$\delta_{ref} = \|\hat{\Gamma} - \hat{\Gamma}_{ref}\| \tag{1.30}$$

and the accuracy of this expression can be expressed as

$$\begin{gathered} f_{\underline{\omega}} = \frac{\delta_{ref} - \delta_{\underline{\omega}}}{\delta_{ref}}, \\ \text{where } 0 \leq f_{\underline{\omega}} \leq 1. \end{gathered} \tag{1.31}$$

Upon being given a molecular wavefunction, Ψ, the Natural Bond Orbital analysis program[31] can extract the optimal natural bond orbitals, Ω_i, for an optimal Lewis-type wavefunction,[32] $\Psi^{(L)}$:

$$\Psi^{(L)} = \det|(\Omega_1)^2(\Omega_2)^2...|. \tag{1.32}$$

Here, Ω_i are doubly occupied natural bond orbitals representing bonds or lone pairs of the formal Lewis structure. The $N/2$-occupied natural bond orbitals, Ω_i, are complemented

by the antibonding and Rydberg set of natural bond orbitals, Ω_j^*. The program provides information on the $\Omega_i \rightarrow \Omega_j$ natural bond orbital interaction that lead to the breakdown of the localized Ψ^L representation of the wave function.

A delocalization list of $\Omega_i \rightarrow \Omega_j$ natural bond orbital interactions of a parent reference structure can be used to generate a list of the associated secondary structures. Second order perturbation theory is then routinely used to calculate the energy of the entries on the natural bond orbital delocalization list. Thus, by selecting an energetic threshold, one may control the number of resonance structures in the expansion.

1.5 Systems of Interest

The first system discussed here is the twisted triplet state ($^3A_1$) of ethylene. Due to difficulties in synthesizing the $^3A_1$ state in appreciable concentrations, experimental studies of the $^3A_1$ state are scarce.[33] However, as the $^3A_1$ state is the lowest energy triplet state of ethylene, it is likely a relevant species in excited electronic state pathways.[34] Additonally, the twisted structure of the $^3A_1$ state provides usefulness as benchmarking compound for synthesizing triplet ground states via schemes where significant steric hindrance will result in near-90° structures.[35] We present structures, anharmonic frequencies, and rotational constants for the C_2H_4, $^{13}C_2H_4$, and C_2D_4 isotopologues of the $^3A_1$ state.

The latter half of this dissertation investigates the Group 15 and Group 16 congeners of OPN. The recent discovery of PN in the oxygen-rich shell of supergiant star VY Canis Majoris points to the formation of isomers of OPN.[36] The linear OPN and ONP structures have nearly degenerate energies and have been a source of debate in the literature.[37,38] While traditional chemical insight points to OPN being lower in energy, the majority of computational studies have predicted ONP to be the lower energy isomer. Herein, we investigate this system using CCSD(T) with basis sets extrapolated to the full basis set limit using focal point analysis. We extend our study to the Group 15 (OPP, OPAs, and OPSb) and Group 16 (SPN, SePN,

and TePN) congeners of OPN. Further, we provide anharmonic frequencies and corrected rotational constants for the potential circumstellar compounds OPN, SPN, and OPP.

Table 1.1: H_2 + CO $\rightarrow$ Formaldehyde

basis set	HF	+δMP2	+δCCSD	+δCCSD(T)	+δCCSDT	+δCCSDT(Q)	NETΔE
cc-pVDZ	-1.01	+1.92	-0.11	-0.51	+0.39	-0.04	[+0.63]
cc-pVTZ	-0.86	+5.28	-0.40	-0.26	[+0.39]	[-0.04]	[+4.12]
cc-pVQZ	-0.85	+6.05	-0.47	-0.14	[+0.39]	[-0.04]	[+4.94]
cc-pV5Z	-0.66	+6.23	-0.51	-0.10	[+0.39]	[-0.04]	[+5.31]
cc-pV6Z	-0.64	+6.29	-0.52	-0.09	[+0.39]	[-0.04]	[+5.39]
CBS Limit	[-0.64]	[+6.38]	[-0.53]	[-0.08]	[+0.38]	[-0.04]	**[+5.49]**

Chapter 2

Twisted Triplet Ethylene: Anharmonic Frequencies and Spectroscopic Parameters for C_2H_4, C_2D_4, and $^{13}C_2H_4$

2.1 Introduction

Small hydrocarbons are ideal species for research in that they have a limited number of degrees of freedom and few low energy conformers, while also exhibiting the complexity of larger molecules, including hyperconjugation and multiple bonding.[39,40] As a prominent member of this set, ethylene gains distinction as the simplest π-bonding molecule and as a prototype system for understanding larger unsaturated systems.[41,42] The stability of ethylene makes it useful for monitoring reactions, especially in kinetics studies where it is used to elucidate the rate constants of radical processes. Fundamental properties of ethylene, such as its rotational barrier, have been studied by experimentalists and theoreticians for decades:[43–50] Crawford and co-workers reported the vibrational spectra of ethylene's ^1A_g ground-state in the 1940s,[51,52] and J. L. Duncan and co-workers carefully studied its vibrational modes[53–62] – reporting the general harmonic forcefield of ethylene in 1973.[63]

Studies regarding the lowest-energy triplet state of ethylene are scarce. This is due, in part, to its transient nature and the difficulty associated with synthesis in appreciable concentrations. Study of the $\tilde{a}\ ^3A_1$ state is further inhibited by its low ultraviolet cross

section, necessitating the use of spectroscopic techniques involving greater sensitivity, such as hemispherical electron spectrometry, high-resolution electron monochromatry, or cavity ring down spectroscopy.[33,64–74] Despite the aforementioned difficulties associated with the $\tilde{a}$ $^3A_1$ spectrum, it has garnered interest partially due to its twisted geometry. As the methylene groups twist, the movement toward a perpendicular structure decreases the π-orbital overlap, transforming the planar D_{2h} structure to the 90 ° D_{2d} structure. For ethylene, the planar excited-state geometry ($^3B_{1u}$) is obtained from vertical excitation; the equilibrium triplet geometry ($^3A_1$) is realized after the structure twists to a lower energy D_{2d} configuration. Further, since studies suggest synthesizing triplet ground states via schemes where significant steric hindrance will result in near 90 ° structures, the $^3A_1$ state also has usefulness as a benchmarking compound for these endeavors.[35]

Notwithstanding the interest in the $\tilde{a}$ $^3A_1$ state, studies of its fundamental properties are not abundant. A. G. Suits and co-workers reported an important measurement on the ethylene adiabatic ($\tilde{X}$ $^1A_g \rightarrow \tilde{a}$ $^3A_1$) energy difference using tunable synchrotron radiation to probe the dissociation dynamics of ethylene sulfide.[45] The groups of Dixon[34] and earlier Peyerimhoff[43] computed both adiabatic and vertical singlet-triplet excitation energies for ethylene. As the $^3A_1$ state is likely a relevant species in excited electronic state pathways, knowledge of its vibrational frequencies is paramount. A theoretical study by Kim and co-workers[75] predicted the harmonic vibrational frequencies of the $\tilde{a}$ $^3A_1$ state, but there is still no report of its anharmonic vibrational frequencies. Fortunately, theory is directly applicable to this system since it is both rigid and small.[75–79]

In this work, we present the anharmonic vibrational frequencies for the $\tilde{a}$ $^3A_1$ state ($1a_1^2 1b_2^2 2a_1^2 2b_2^2 1e_x^2 1e_y^2 3a_1^2 2e_x^1 2e_y^1$) of ethylene, C_2H_4, and two of its isotopologues, $^{13}C_2H_4$ and C_2D_4, computed at the CCSD(T) level of theory with the cc-pVQZ basis set. No experimental or theoretical reports of the anharmonic vibrational frequencies for C_2H_4 and its isotopologues have been published to date. Our research thus gives the first complete set of

anharmonic frequencies for twisted triplet ethylene. Additionally, we also offer parameters pertinent to other spectroscopic measurements, including the optimized geometries (r_e and r_g) and rotational constants (B_e and B_0) for the three isotopologues.

2.2 Methods

The geometric parameters of the twisted structure of triplet ethylene were fully optimized here using coupled-cluster theory with single, double, and perturbative triple excitations [CCSD(T)].[80–85] We used Dunning's correlation-consistent cc-pVQZ basis set,[86] which contains 230 contracted spherical harmonic Gaussian functions. All computations were carried out using the Cfour[87] program package. An unrestricted Hartree-Fock (UHF) reference was adopted because of the open-shell character of the triplet state. A small amount of spin contamination ($\langle\, \widehat{S}^{\,2} \,\rangle \leq 2.015$) was encountered, which supports this choice. We note that it has been previously shown that spin contamination in the reference wavefunction is often diminished by subsequent coupled-cluster computations.[88,89] Also, no instabilities were detected in the UHF wavefunction. Analytic second derivatives[90,91] were utilized in frequency computations.

Since the cc-pVQZ basis set does not include a description of core electron correlation, the lowest energy 1*s*-like molecular orbitals of carbon are frozen in the correlation computations. In order to gauge the error introduced by using this "frozen core" approximation, we computed the harmonic vibrational frequencies of the three isotopologues using the CCSD(T)/cc-pCVQZ method (288 contracted spherical harmonic Gaussian functions) and compared it to the CCSD(T)/cc-pVQZ computations. The results are collated in Table 2.1. We find that the addition of core correlation effects resulted in an at most +0.5% difference in the vibrational frequencies of triplet ethylene. Additionally, our choice to use a basis set without core correlation is supported by research that has shown that the addition of core

electron correlation without the inclusion of quadruple excitations results in a misleading blue shift of the harmonic vibrational frequencies.[92–94]

Second order vibrational perturbation theory (VPT2)[95] was used in the frequency computations in order to take into account the anharmonic nature of the potential energy surface. Numerical differentiation of second derivatives at 15 nuclear displacements was used to generate the requisite cubic and semidiagonal quartic force fields. Analytic derivatives computed at the CCSD(T)/cc-pVQZ level of theory were utilized. During VPT2 analysis, corrections were made for the C_2D_4 species in order to treat Fermi-Dennison resonances.[46] Note, discussion of the problematic anharmonic corrections for the wagging modes are analyzed in the final section of this paper.

2.3 Results and Discussions

2.3.1 Structures and energetics

Figure 2.1 shows a depiction of the equilibrium structure of the lowest triplet state of C_2H_4 ($\tilde{a}\ ^3A_1$, D_{2d} symmetry) computed at the CCSD(T)/cc-pVQZ level of theory. The optimized equilibrium geometric parameters (r_e) are shown in Table 2.2 along with the r_g values, discussed below, that include vibrational corrections.[96–98]

We predict C_2H_4 to have an equilibrium C−C bond length of 1.453 Å. Compared to the C−C single bond length in ethane (1.533 Å)[99] and the C−C double bond length in singlet ethylene (1.334 Å), the computed C−C bond length in triplet ethylene is approximately halfway between them, though closer to the former, which suggests some vestige of a π orbital. Wu and Schleyer[100] proposed that hyperconjugation exists between the σ orbitals of C−H bond and the p orbitals on the opposite carbon atom, which could probably compensate for the substantial, but not complete, loss of π conjugation. The rough equivalence of the equilibrium C−H bond in triplet ethylene (1.084 Å) and singlet ethylene (1.082 Å) reveals the

small influence on the C−H σ bond from the drastic change in C−C π bonding. Similarly, the $\angle$ H−C−C bond angle (121.5 °) shows minor distortion from the geometry of singlet ethylene (121.4 °). We note, for reference, that the parameters of our equilibrium structure agree well with the quantum Monte Carlo work of Barborini and co-workers.[44]

The equilibrium geometry (r_e) for the ^{13}C- and deuterium-substituted isotopologues are equivalent to the parent species. Corrections for thermal vibrations, which are dependent on the atomic masses, yield an r_g structure that differs among the three species (see Kuchitsu, reference [96], for definitions). Using the normal coordinates, r_g may be expressed as[97,98]

$$\begin{aligned} r_g &= r_e + \sum_s \gamma_s \langle Q_s \rangle + \frac{1}{2} \sum_{st} \gamma_{st} \langle Q_s Q_t \rangle + ... \\ &\approx r_e + \sum_s \gamma_s \langle Q_s \rangle + \frac{1}{2} \sum_s \gamma_{ss} \langle Q_s^2 \rangle \end{aligned} \tag{2.1}$$

where γ_s and γ_{st} are the first and second derivatives of the internuclear distances with respect to the corresponding normal coordinates. At 0 Kelvin, the linear average $\langle Q_r \rangle$ and quadratic average $\langle Q_s^2 \rangle$ on the right-hand side of (2.1) are computed using the formulae

$$\begin{aligned} \langle Q_r \rangle &= -\left(\frac{\hbar}{2\pi c \omega_r^3} \right)^{\frac{1}{2}} \sum_s \phi_{rss} \\ \langle Q_s^2 \rangle &= \frac{\hbar}{4\pi c \omega_s} \end{aligned} \tag{2.2}$$

where ω_r is the harmonic frequency of the rth mode and ϕ_{rss} is a cubic force constant. Note that both ω and ϕ in (2.2) depend on the nuclear masses, yielding different zero-point corrected geometries for the three isotopologues. Relative to the r_e structure, C−C bonds are increased by 0.0086 Å or more and the C−H bonds by 0.0152 Å or more. The latter bonds are strongly affected due to the high degree of anharmonicity along those coordinates (vide infra). Table 2.2 also shows that the bond lengths of the r_g structures are always

longer than those of the equilibrium geometry, which is consistent with the general features of vibrationally-averaged structures.

2.3.2 Vibrational frequencies

The twelve normal vibrational modes of triplet ethylene and their symmetries are described in Table 2.3. The D_{2d} symmetry makes all vibrational modes Raman active with $v_5 - v_{12}$ being infrared (IR) active. Due to the fleeting nature of triplet C_2H_4, neither the Raman or IR spectroscopy has been observed experimentally. Therefore, our predicted vibrational frequencies may provide assistance to future experimental world.

In Table 2.4−2.6, we list our computed harmonic and anharmonic vibrational frequencies for triplet C_2H_4 and its isotopologues. These results show that the anharmonic frequencies are generally lower than the harmonic predictions by about 3.2 %, except for the two wagging modes with lowest frequencies (v_{11} and v_{12}). More discussion of the large anharmonic corrections for v_{11} and v_{12}, which we consider to be unphysical, is given in a later section.

$\mathbf{C_2H_4}$

Vibrational frequencies and IR intensities for the parent molecule are reported in Table 2.4. Compared to the scaled harmonic vibrational frequencies obtained theoretically by Kim and co-workers, most differencies are approximately 2.0 % except for v_{11} and v_{12}, which differ by around 20 %, as mentioned. Note that Kim and co-workers report harmonic frequencies scaled by a factor of 0.9776. For most vibrational modes, such scaled frequencies lie between our corresponding harmonic and anharmonic frequencies, closer to the latter for v_3, v_4, v_9 and v_{10}, while slightly closer to the former for the rest. The IR intensity of the CH_2 in-plane scissoring mode, v_6, is predicted to be relatively low, which may prohibit observation of this particular vibration in future experiments. The most intense vibrational modes are found to be the out-of-plane wagging vibration of the two CH_2 terminal groups, v_{11} and v_{12}.

$^{13}C_2H_4$

Vibrational frequencies and IR intensities for $^{13}C_2H_4$ are reported in Table 2.5. As for the parent isotopologue, the anharmonic corrections and IR intensities for $^{13}C_2H_4$ reveal a distinct pattern. From Table 2.7, isotopic shifts of the anharmonic frequencies with respect to the parent molecule for all vibrational modes may be inspected. All frequencies are reduced in magnitude, with the C−C stretching mode v_3 affected most (3.1 %) by ^{13}C isotopic substitution. The CH_2 in-plane rocking, v_9 and v_{10}, shift 1.0 % because they also involve vibration of the carbon atoms. As expected, the CH_2 out-of-plane twisting mode, v_4, remains nearly unchanged (0.01 %) by ^{13}C substitution.

C_2D_4

Vibrational frequencies and IR intensities for C_2D_4 are reported in Table 2.6. Deuterium substitution results in a considerable shift (¿ 17 %) for all vibrational modes, with respect to the parent molecule. This is, of course, due to the relative mass change arising from deuterium substitution. The CH_2 out-of-plane twisting mode, v_4, which involves only vibrations of hydrogen atoms, suffers the most significant reduction (upon deuteration) in magnitude, 28 %. Note that v_4 was the mode least affected by ^{13}C isotopic substitution in the case of $^{13}C_2H_4$.

Our VPT2 analyses were generally free from problematic Fermi-Dennison resonances. The v_5 vibrational mode of C_2D_4 suffers from a Fermi type II resonance, however, when perturbed by the modes v_2 and v_6 ($\omega_2 + \omega_6 \approx \omega_5$). As is the standard procedure, first proposed by Nielsen,[101] we remove the contributions with small denominators from the

summations in the VPT2 analyses, and estimate the energetic effect of neglecting such items via the first-order couplings:

$$\begin{pmatrix} \omega_2 + \omega_6 & \phi_{2,5,6}/\sqrt{8} \\ \phi_{2,5,6}/\sqrt{8} & \omega_5 \end{pmatrix} \tag{2.3}$$

where ϕ_{ijk} is the cubic force constant with respect to the modes i, j, and k. It is straightforward to consider the diagonal terms to be the zero-order states and the off-diagonal terms to represent a first-order perturbation. Denoting the separation between $\omega_2 + \omega_6$ and ω_5 by Δ, it may be shown that the eigenvalues of the matrix (2.3) are given by:

$$v = \omega_5 + \frac{\Delta}{2}\left(1 \pm \sqrt{1 + \frac{\phi_{2,5,6}^2}{2\Delta^2}}\right) \tag{2.4}$$

Our final v_5 prediction is obtained by adding a correction, which is the difference between the desired eigenvalue computed from (2.4) and ω_5, compared to the deperturbed v_5. This eigenvalue of (2.3) corresponds to an eigenvector containing the maximal ω_5 content. The resulting value is 2156.5 cm^{-1}, 16.9 cm^{-1} lower than the deperturbed frequency.

Rotational constants

Rotational constants for the equilibrium and vibrationally averaged structures of the species under study are shown in Table 2.8. Such corrections arise from two sources: vibrational zero-point effects and quartic centrifugal distortion effects. Including vibrational zero-point effects alone yields A_0, B_0, and C_0, while the inclusion of both effects gives A', B', and C'.

To second order, the molecular rotational constant B_0 for the vibrational ground state is related to the equilibrium rotational constant B_e by[102]

$$B_0 \approx B_e - \frac{1}{2}\sum_r \alpha_r^B + \cdots \tag{2.5}$$

where α_r^x (x = A, B, or C) denotes the vibration-rotation interaction constants, which describe the coupling of rotations about the principal axis x with the normal mode r. Further, taking into account the quartic centrifugal distorsion constants $\tau_{\alpha\beta\gamma\delta}$, one may obtain the effective rotational constant B' (which corresponds to the Hamiltonian used to fit the observed energy levels) via[103]

$$B' = B_0 + \frac{1}{4}(3\tau_{caca} - 2\tau_{abab} - 2\tau_{bcbc}) \tag{2.6}$$

The zero-point effects (Eq. 2.5) provide the most significant corrections, lowering $\{A_e, B_e, C_e\}$ by {2181.7, 122.6, 122.6} MHz, respectively, for the parent isotopologue, C_2H_4. The quartic centrifugal distortion effects (Eq. 2.6) contribute minimally, further reducing $\{A_0, B_0, C_0\}$ by {-0.70, 0.17, 0.17} MHz. The corrected rotational constants are lower than their equilibrium counterparts by {1.5, 0.5, 0.5}%, consistent with the bond elongation observed in the vibrationally averaged structure, relative to the equilibrium structure. Similar trends are observed for the other two isotopologues.

2.4 Challenges from the anharmonicity of the wagging modes

As reported in Table 2.4−2.6, the wagging modes, v_{11} and v_{12}, of triplet C_2H_4, $^{13}C_2H_4$ and C_2D_4 involve large anharmonic corrections to the vibrational frequencies (+24.9 % on average) compared to those of other modes (−3.2 % on average). There may be several possible explanations for this behavior. First, as a symmetric top molecule, twisted triplet ethylene with D_{2d} point group allows for degenerate frequencies whose complexity[104] might not be treated properly by the VPT2 module in Cfour. To evaluate this possibility, the molecular symmetry may be lowered by either replacing one hydrogen with deuterium, or by changing the mass of one hydrogen by a small amount, yielding an asymmetric top molecule. Table 2.9 compares harmonic and anharmonic frequencies of the wagging modes for triplet C_2H_4,

C_2H_3H', and C_2H_3D, where C_2H_3H' is a molecule containing a hypothetical atom, H′, that has 1% larger mass than hydrogen. Here we can see that the results of two symmetry-broken molecules have similar anharmonic corrections as in the parent molecule, which refutes our first hypothesis. In 2001, Auer and Gauss[105] reported anharmonic frequencies for allene, which also has a D_{2d} symmetry and is a symmetric top, using the VPT2 method implemented in CFOUR. We obtained a set of allene anharmonic frequencies in good agreement with the experimental frequencies[106] and the theoretical results from Auer and Gauss. Table 2.10 compares the results obtained by the different methods. For the wagging modes of allene, v_3 and v_4, our anharmonic corrections at the CCSD(T)/cc-pVTZ level of theory diminish the deviation from experimental frequencies to -3.1 cm^{-1}. The computations on allene, along with our results for C_2H_3H' and C_2H_3D preclude the degenerate vibrations of the wagging modes as a possible problem.

Other errors could arise from the finite difference technique that is utilized to obtain cubic and quartic force constants from second derivatives computations at displacements from the equilibrium geometry. Values for the displacement size along the normal coordinates must be large enough to capture the vibrational motion, but small enough to be local to the equilibrium region. As such, it is possible that to capture the nature of the potential energy surface for the wagging modes larger or smaller displacement values are needed. Table 2.11 shows the anharmonic vibrational corrections of the wagging modes with respect to the displacement size. Varying the displacement value does not noticeably affect the anharmonic corrections of the wagging modes, however. In fact, the displacements in the finite difference method are less crucial to the wagging modes than to the stretching or bending, because the region of the potential energy surface for the former appears to be much flatter than that of the latter.

Thirdly and perhaps most problematically, the quartic force constants of the wagging modes are arrestingly larger than those for the other modes. With inspection of the con-

tribution to the anharmonic frequencies and constants (the relevant equations are detailed in reference [46]), the largest positive component of the anharmonic corrections derives from the self-couplings, $\chi_{11,11}$ and $\chi_{12,12}$, and inter-couplings, $\chi_{11,12}$ of the two wagging modes. For these the largest positive contributor comes from the quartic force constants, $\phi_{11,11,11,11}$, $\phi_{11,11,12,12}$, $\phi_{12,12,11,11}$ and $\phi_{12,12,12,12}$. The VPT2 method, which starts from the harmonic-oscillator rigid-rotator approximation, cannot be reliably applied to modes where the quadratic terms do not dominate the potential energy surface.

To summarize this section, we have analyzed issues arising from the symmetric top nature of the molecule and the influence of displacement increments as possible explanations to the unacceptable anharmonic corrections to the wagging modes. A rational candidate among possible reasons for the failure of the VPT2 method when applied to the wagging modes of triplet ethylene appears to be the absence of a dominant harmonic term for the potential.

2.5 Conclusions

The lowest triplet-state ($\tilde{a}\ ^3A_1$) of C_2H_4 is of both theoretical and experimental interest. In the present research, we have focused on the structure and vibrational modes of this electronic state of twisted C_2H_4 and its two isotopologues using the CCSD(T)/cc-pVQZ level of theory. With VPT2 theory, we have also studied the zero-point corrected structures and fundamental vibrational frequencies. This is the first time the anharmonic frequencies of the ten vibrational modes for triplet ethylene (and two of its isotopologues) have been predicted. We hope this research will provide guidance for future experimental investigations of triplet ethylene.

2.6 Tables

Table 2.1: Harmonic vibrational frequencies (in cm^{-1}) for triplet ethylene isotopologues with IR intensities (in km/mol, listed parenthetically) predicted by the frozen-core method and the all-electron correlated method.

	C_2H_4		$^{13}C_2H_4$		C_2D_4	
Mode	Frozen[a]	All-electron[b]	Frozen[a]	All-electron[b]	Frozen[a]	All-electron[b]
v_1	3115.4 (0.0)	3121.2 (0.0)	3110.1 (0.0)	3115.8 (0.0)	2261.9 (0.0)	2266.1 (0.0)
v_2	1465.7 (0.0)	1468.3 (0.0)	1456.1 (0.0)	1458.5 (0.0)	1220.8 (0.0)	1224.7 (0.0)
v_3	1135.1 (0.0)	1139.4 (0.0)	1099.5 (0.0)	1103.8 (0.0)	939.3 (0.0)	941.4 (0.0)
v_4	693.7 (0.0)	696.5 (0.0)	693.7 (0.0)	696.5 (0.0)	490.7 (0.0)	492.7 (0.0)
v_5	3119.8 (18.5)	3125.7 (17.7)	3114.9 (18.4)	3120.8 (17.7)	2252.1 (9.5)	2256.4 (9.1)
v_6	1439.7 (0.1)	1442.5 (0.2)	1434.0 (0.1)	1436.8 (0.2)	1067.2 (0.1)	1069.2 (0.1)
v_7	3207.6 (5.3)	3213.4 (5.0)	3194.5 (5.2)	3200.3 (4.9)	2387.4 (3.5)	2391.7 (3.3)
v_8	3207.6 (5.3)	3213.4 (5.0)	3194.5 (5.2)	3200.3 (4.9)	2387.4 (3.5)	2391.7 (3.3)
v_9	939.7 (1.2)	942.3 (1.2)	930.5 (1.0)	933.1 (1.0)	739.4 (2.6)	741.8 (2.6)
v_{10}	939.7 (1.2)	942.3 (1.2)	930.5 (1.0)	933.1 (1.0)	739.4 (2.6)	741.8 (2.6)
v_{11}	407.6 (53.8)	414.1 (54.4)	404.6 (53.1)	411.1 (53.7)	311.7 (31.1)	316.5 (31.5)
v_{12}	407.6 (53.8)	414.1 (54.4)	404.6 (53.1)	411.1 (53.7)	311.7 (31.1)	316.5 (31.5)

[a] Computed at the CCSD(T)/cc-pVQZ level of theory with frozen core.
[b] Computed at the CCSD(T)/cc-pCVQZ level of theory with core correlation.

Table 2.2: Structural parameters (in Å and degrees) for selected isotopologues of triplet ethylene molecules.

		Zero-point corrected[a]			
Parameter	r_e	C_2H_4	$^{13}C_2H_4$	C_2D_4	Ref.[44][b]
r(C−C)	1.4528	1.4620	1.4617	1.4614	1.4556
r(C−H)	1.0838	1.1045	1.1044	1.0990	1.0820
$\angle$ H−C−C	121.49	120.18	120.19	120.45	121.48

[a] Computed at the CCSD(T)/cc-pVQZ level of theory.
[b] Variational Monte Carlo with a smooth relativistic norm-conserving pseudopotential; C_2H_4 isotopologue.

Table 2.3: Descriptions and symmetries for the vibrational modes of triplet C_2H_4.

Mode	Description	Symmetry
v_1	CH_2 symmetric stretching	a_1
v_2	CH_2 in-plane scissoring	a_1
v_3	CC stretching	a_1
v_4	CH_2 out-of-plane twisting	b_1
v_5	CH_2 symmetric stretching	b_2
v_6	CH_2 in-plane scissoring	b_2
v_7	CH_2 antisymmetric stretching	e
v_8	CH_2 antisymmetric stretching	e
v_9	CH_2 in-plane rocking	e
v_{10}	CH_2 in-plane rocking	e
v_{11}	CH_2 out-of-plane wagging	e
v_{12}	CH_2 out-of-plane wagging	e

Table 2.4: Harmonic and anharmonic vibrational frequencies (in cm^{-1}) for triplet twisted C_2H_4 with IR intensities (in km/mol, listed parenthetically).

	This research[a]		Previous research
Mode	Harmonic	Anharmonic	Ref.[75] [b]
v_1	3115.4 (0.0)	2978.2 (0.0)	3060.6
v_2	1465.7 (0.0)	1426.8 (0.0)	1449
v_3	1135.1 (0.0)	1103.7 (0.0)	1109.6
v_4	693.7 (0.0)	651.2 (0.0)	662.2
v_5	3119.8 (18.5)	2982.4 (16.8)	3062.7
v_6	1439.7 (0.1)	1403.8 (0.5)	1424.3
v_7	3207.6 (5.3)	3050.0 (6.2)	3150
v_8	3207.6 (5.3)	3050.0 (6.2)	3150
v_9	939.7 (1.2)	925.7 (2.0)	925.6
v_{10}	939.7 (1.2)	925.7 (2.0)	925.6
v_{11}	407.6 (53.8)	516.0 (36.8)	339.4
v_{12}	407.6 (53.8)	516.0 (36.8)	339.8

[a] Computed at the CCSD(T)/cc-pVQZ level of theory.

[b] Computed at the QCISD/6−311G(d,p) level of theory and scaled by the factor 0.9776.

Table 2.5: Harmonic and anharmonic vibrational frequencies (in cm^{-1}) for triplet twisted $^{13}C_2H_4$ with IR intensities (in km/mol, listed parenthetically).

	This work[a]	
Mode	Harmonic	Anharmonic
v_1	3110.1 (0.0)	2972.6 (0.0)
v_2	1456.1 (0.0)	1418.8 (0.0)
v_3	1099.5 (0.0)	1070.8 (0.0)
v_4	693.7 (0.0)	651.0 (0.0)
v_5	3114.9 (18.4)	2977.3 (16.6)
v_6	1434.0 (0.1)	1397.3 (0.5)
v_7	3194.5 (5.2)	3040.2 (6.0)
v_8	3194.5 (5.2)	3040.1 (6.0)
v_9	930.5 (1.0)	916.2 (1.7)
v_{10}	930.5 (1.0)	916.2 (1.7)
v_{11}	404.6 (53.1)	513.4 (35.8)
v_{12}	404.6 (53.1)	513.3 (35.9)

[a] Computed at the CCSD(T)/cc-pVQZ level of theory.

Table 2.6: Harmonic and anharmonic vibrational frequencies (in cm^{-1}) for triplet twisted C_2D_4 with IR intensities (in km/mol, listed parenthetically).

	This work[a]	
Mode	Harmonic	Anharmonic
v_1	2261.9 (0.0)	2181.8 (0.0)
v_2	1220.8 (0.0)	1191.9 (0.0)
v_3	939.3 (0.0)	919.9 (0.0)
v_4	490.7 (0.0)	469.1 (0.0)
v_5	2252.1 (9.5)	2173.4 (9.0)
v_6	1067.2 (0.1)	1051.0 (0.1)
v_7	2387.4 (3.5)	2300.0 (3.9)
v_8	2387.4 (3.5)	2300.0 (3.9)
v_9	739.4 (2.6)	733.7 (3.2)
v_{10}	739.4 (2.6)	733.7 (3.2)
v_{11}	311.7 (31.1)	376.3 (23.0)
v_{12}	311.7 (31.1)	376.3 (23.0)

[a] Computed at the CCSD(T)/cc-pVQZ level of theory.

Table 2.7: Triplet ethylene isotopic vibrational shifts (in cm^{-1}) with respect to the parent isotopologue C_2H_4.

Mode	$^{13}C_2H_4$	C_2D_4
v_1	−5.6	−804.8
v_2	−8.1	−234.9
v_3	−32.9	−183.8
v_4	−0.2	−182.2
v_5	−5.0	−800.6
v_6	−6.5	−352.7
v_7	−9.8	−750.0
v_8	−9.8	−750.0
v_9	−9.6	−192.1
v_{10}	−9.6	−192.1
v_{11}	−2.6	−139.6
v_{12}	−2.6	−139.6

Table 2.8: Twisted triplet ethylene rotational constants (in MHz) from the equilibrium geometry, and with vibrational zero-point corrections (in MHz).

Parameter	C_2H_4	$^{13}C_2H_2$	C_2D_4
A_e	146761.9	146761.9	73437.4
B_e	23928.8	22786.4	17094.9
C_e	23928.8	22786.4	17094.9
A_0	144580.7	144559.8	72741.2
B_0	23806.3	22669.2	17036.7
C_0	23806.3	22669.2	17036.7
A'	144581.4	144560.4	72741.5
B'	23806.1	22669.0	17036.6
C'	23806.1	22669.0	17036.6

Table 2.9: Harmonic and anharmonic vibrational frequencies (in cm^{-1}) of wagging modes for the C_2H_4, C_2H_3H', and C_2H_3D isotopomers[a] of twisted triplet ethylene.

	C_2H_4		C_2H_3H'[b]		C_2H_3D	
Mode	Harm.	Anharm.	Harm.	Anharm.	Harm.	Anharm.
v_{11}	407.6	516.0	401.3	512.1	352.7	439.9
v_{12}	407.6	516.0	402.0	512.9	397.6	507.0

[a] The results for C_2H_3H' and C_2H_3D are both computed at the CCSD(T)/cc-pVTZ level of theory.

[b] The mass of H′ is 1% greater than that of hydrogen.

Table 2.10: Theoretical harmonic and fundamental frequencies (in cm^{-1}) of allene C_3H_4 compared with experiment.

Mode	Symmetry	Harmonic[a]	Fundamental[a]	Auer and Gauss.[b]	Experiment[c]
v_1	e	348.0	348.2	351	352.73
v_2	e	348.0	348.2	351	
v_3	e	856.7	837.8	851	840.93
v_4	e	856.7	837.8	851	
v_5	b_1	870.3	849.3	857	848.59
v_6	e	1017.8	997.9	1005	999.00
v_7	e	1017.8	997.9	1005	
v_8	a_1	1080.8	1067.2	1078	1072.22
v_9	b_2	1438.4	1395.2	1411	1359.0
v_{10}	a_1	1488.6	1441.5	1457	1442.55
v_{11}	b_2	2012.2	1953.5	1985	1959.1
v_{12}	a_1	3142.8	3011.3	3040	3006.7
v_{13}	b_2	3144.3	3015.7	3044	
v_{14}	e	3226.4	3078.7	3096	3085.43
v_{15}	e	3226.4	3078.7	3096	

[a] Harmonic frequencies computed at CCSD(T)/cc-pVTZ with anharmonic correction computed at the same level of theory as well.

[b] Harmonic frequencies computed at CCSD(T)/cc-pVTZ with anharmonic correction computed at MP2/cc-pVTZ. See reference [105].

[c] See reference [106].

Table 2.11: Anharmonic vibrational corrections (in cm^{-1}) of wagging modes for triplet C_2H_3H' with respect to values of the displacement (in terms of reduced normal coordinates).[a]

	Displacement			
Mode	0.050	0.060	0.075	0.100
v_{11}	+112.5	+109.8	+111.0	+110.8
v_{12}	+107.2	+110.4	+110.6	+110.9

[a] Computed at the CCSD(T)/cc-pVTZ level of theory.

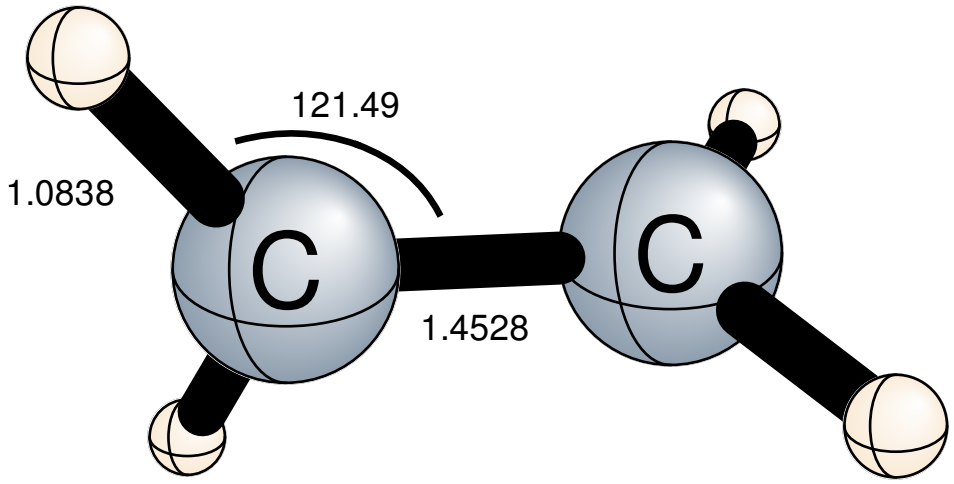

Figure 2.1: The equilibrium geometry (in Å and degrees) of 90 °-twisted triplet ethylene, possessing D_{2d} symmetry, computed at the CCSD(T)/cc-pVQZ level of theory.

Chapter 3

Structures, Bonding, and Energetics of Potential Triatomic Circumstellar Molecules Containing Group 15 and 16 Elements [1]

[1] W. E. Turner II, J. Agarwal, and H. F. Schaefer III *J. Phys. Chem. A*, **2015**, 119, 1. Reprinted here with permission of the American Chemical Society.

3.1 Abstract

The recent discovery of PN in the oxygen-rich shell of the supergiant star VY Canis Majoris points to the formation of several triatomic molecules involving oxygen, nitrogen, and phosphorus; these are also intriguing targets for main-group synthetic inorganic chemistry. In this research, high-level *ab initio* electronic structure computations were conducted on the potential circumstellar molecule OPN and several of its heavier Group 15 and 16 congeners (SPN, SePN, TePN, OPP, OPAs, and OPSb). For each molecule, four isomers were examined. Optimized geometries were obtained with coupled cluster theory [CCSD(T)] using large Dunning basis sets [aug-cc-pVQZ, aug-cc-pV(Q+d)Z, and aug-cc-pVQZ-PP], and relative energies are reported at the complete basis set limit of CCSDT(Q) from focal point analyses. The linear phosphorus-centered molecules were consistently the lowest in energy of the Group 15 congeners by at least 6 kcal mol^{-1}, resulting from double-triple and single-double bond resonances. The linear nitrogen-centered molecules were consistently the lowest in energy of the Group 16 congeners by at least 5 kcal mol^{-1}, due to the electronegative central nitrogen atom encouraging electron delocalization throughout the molecule. For OPN, OPP, and SPN, anharmonic vibrational frequencies and vibrationally corrected rotational constants are predicted; good agreement with available argon matrix values is observed.

3.2 Introduction

In the past three decades, an increasing number of molecules containing second row elements have been identified in the clouds of stars.[107–113] Molecules containing phosphorus and sulfur, in particular, have been observed in stardust grains, star-forming regions, and within the clouds of circumstellar shells.[114–123] In oxygen-rich environments, these atoms often react to form oxides of one to three atoms, with reactions progressing both in the gas phase and on stardust grains.[36] In the latter case, the grain surface serves to promote small molecule

formation as adsorbed atoms form molecules through particle bombardment and cosmic ray irradiation.[124] These oxygen-rich granular environments may produce several phosphorus and sulfur oxides such as PO, SO, and SO_2 by means of neutral-neutral and ion-molecule processes with H and OH radicals.[125,126] In contrast, PN is generated in carbon-rich settings from the reaction of phosphorus atoms with HCN.[127] However, a 2007 study by Ziurys and coworkers reported the first observance of PN in the oxygen-rich shell of the supergiant star VY Canis Majoris.[36]

The discovery of PN in an oxygen-rich cloud strongly suggests that triatomics of O, P, and N, also exist. ONP is indeed a somewhat stable molecule that was first isolated in terrestrial laboratories in 1988 and characterized with infrared spectroscopy.[128,129] Okabayashi and coworkers[130] later reported the microwave spectrum of $^{16}O^{14}NP$ and its isotopomers $^{16}O^{15}NP$ and $^{18}O^{14}NP$ to yield r_s geometric parameters. Tessier and Navrotsky[131] separately determined the enthalpy of formation using high-temperature solution calorimetry, and in 1990, Davy and Schaefer utilized theory to predict the energy difference [ΔE(0 K)] between ONP and OPN; the former was found to be 5 kcal mol^{-1} lower in energy from configuration interaction single and doubles (CISD) computations with the TZ2P basis set.[37]

Traditional chemical insight would not place ONP lower than OPN—one would expect the phosphorus atom, being the least electronegative, to assume the central position in order to encourage charge delocalization. Almost two decades after the initial theory work, Dixon and Francisco championed the traditional insight and found OPN to be 1.7 kcal mol^{-1} lower in energy [ΔE(0 K)] than ONP. Their computations improved upon those of Davy by utilizing coupled cluster theory with single, double, and perturbative triple excitations [CCSD(T)], including extrapolation to the complete basis set (CBS) limit.[38,132] A 2011 article by Zeng *et al.* reported the first matrix isolation of OPN, including OPN to ONP interconversion using UV spectroscopy.[133] The authors also expanded the scope of their study to the sulfur congeners. Notably, they were able to isolate SPN, SNP, and cyclic PSN in argon matrices.

From computations at the CCSD(T)/cc-pVTZ level of theory, they determined that SNP was 17.4 kcal mol^{-1} lower in energy than SPN, which is the opposite energy ordering of OPN and ONP.[134] This shift in ordering engenders questions regarding the underlying changes in electronic structure.

Electronic structure theory is well-suited for examining circumstellar systems, especially given the difficulty inherent in reproducing astral environments in the laboratory.[135–139] Moreover, the large number of species present in circumstellar media often yields overlapping spectral features, which may be disentangled using accurate vibrational predictions.[140] In the current research, the structure, bonding, and relative thermodynamic stability of select Group 15 (OPP, OPAs, and OPSb) and Group 16 (SPN, SePN, and TePN) congeners of OPN is examined. Relative energies of these molecules are reported at the complete basis set limit of CCSDT(Q) from focal point analysis. Harmonic vibrational frequencies are presented for of all of the aforementioned molecules, with anharmonic frequencies and vibrationally-corrected rotational constants included for the isomers of OPN, SPN, and OPP. These predictions should allow for better comparison to existing sparse experimental results. In total, the inclusion of elements in the third and fourth rows of the periodic table offers insight into the bonding of lesser studied elements in the context of ones more prevalent in chemical literature.

3.3 Theoretical Methods

Geometric parameters were optimized using coupled cluster theory with single, double, and perturbative triple excitations [CCSD(T)].[141–144] To describe the nitrogen and oxygen atoms, Dunning's augmented correlation-consistent valence basis sets [aug-cc-pVXZ (X = D, T, Q)][145] were employed. The aug-cc-pV(X+d)Z series of basis sets were used for phosphorus and sulfur since the aug-cc-pVXZ basis sets poorly describe core polarization effects and valence orbital correlation effects in second row atoms.[146–150] For the third and fourth row

atoms, the basis sets and corresponding effective core potentials of Peterson *et al.* were employed (aug-cc-pVXZ-PP).[151,152] Herein, we refer to basis sets generally as AVXZ, noting that the actual basis set corresponds to the appropriate one for that element as determined above.

Harmonic vibrational frequencies were computed using CCSD(T)/AVQZ and can be found on page S1 of the Supporting Information. For better comparison to experimental values, second-order vibrational perturbation theory (VPT2)[95] was used to compute anharmonic corrections to the vibrational frequencies for OPN, SPN, and OPP. For VPT2 computations, coupled cluster theory and the ANO2 atomic natural orbital basis set of Almlöf and Taylor[153,154] were utilized. Specifically, harmonic frequencies were computed at CCSD(T)/ANO2, and then VPT2 anharmonic corrections computed with the same method were appended. Numerical differentiation of second derivatives at six distinct nuclear displacements was used to generate the necessary cubic and semi-diagonal quartic force fields for this analysis. The largest vibrational intensity for each molecule was normalized to 100; the intensities of the remaining modes were scaled accordingly.

To obtain accurate relative energies, focal point analyses were conducted on all of the reported molecules in accordance with the method prescribed by Allen and coworkers.[155–160] Note that all single-point energies were computed using CCSD(T)/AVQZ geometries. The Hartree-Fock energy was extrapolated according to the formula

$$E_x^{\mathrm{HF}} = E_{\mathrm{CBS}}^{\mathrm{HF}} + ae^{-bX}. \tag{3.1}$$

In Eq. 1, X is the cardinal number (i.e., 2 for AVDZ, 3 for AVTZ, and 4 for AVQZ) of the basis, and values a and b are fitting parameters. A two point equation

$$E_x^{\mathrm{corr}} = E_{\mathrm{CBS}}^{\mathrm{corr}} + aX^{-3} \tag{3.2}$$

was used to extrapolate the correlation energy; a is a fitting parameter.

Zero-point vibrational energy (ZPVE) contributions (Δ_{ZPVE}) were appended to the extrapolated energies; anharmonic ZPVE corrections were used for the isomers of OPN, SPN, and OPP.[??] The effect of core correlation (Δ_{core}) was evaluated at the CCSD(T)/cc-pCVTZ level of theory, with aug-cc-pCV(T+d)Z used for phosphorus and sulfur. The correction to scalar relativistic effects, including mass-velocity and Darwin one-electron terms, (Δ_{rel}) and diagonal Born-Oppenheimer effects (Δ_{DBOC}) were computed with HF/AVTZ. The final energies at 0 K are given as

$$\begin{aligned}\Delta \mathrm{E_{0K}} = \quad & \Delta \mathrm{E_{HF}} + \delta\mathrm{MP2} + \delta\mathrm{CCSD} + \delta\mathrm{CCSD(T)} + \delta\mathrm{CCSDT} + \delta\mathrm{CCSDT(Q)} \\ & + \Delta_{\mathrm{core}} + \Delta_{\mathrm{ZPVE}} + \Delta_{\mathrm{rel}} + \Delta_{\mathrm{DBOC}}. \end{aligned} \tag{3.3}$$

Here, ΔE represents a relative energy, and δ denotes incremental changes in ΔE with respect to the preceding level of theory. As is common practice, the Δ_{core} and Δ_{DBOC} corrections are omitted for molecules containing As, Sb, Se, and Te where effective core potentials are employed.[161]

Natural Bond Orbital (NBO) analyses were performed using the NBO 6.0 package[162] interfaced with ORCA.[163] NBO results include Natural Resonance Theory (NRT)[29,164,165] and Wiberg Bond Index (WBI)[166] data. The former (NRT) provides properties from a weighted average of first-order density matrices, while WBI yields the number of electrons involved in a given bond, and thus a quantum-mechanical analog for bond order.[167] The B3LYP[168,169] density functional and the Def2-TZVP basis set[170] were used for these computations. CFOUR 1.0[87] was used for all geometry optimizations, harmonic frequency computations, and anharmonic frequency computations. CCSDT and CCSDT(Q) computations were performed using the string-based quantum chemistry code (MRCC) of Kállay,[171,172] as interfaced with CFOUR.

3.4 Results and Discussion

For each of the Group 15 congeners we considered four isomers containing phosphorus, oxygen, and the Group 15 element: the cyclic isomer and the three linear isomers. Likewise, for each of the Group 16 isomers, we considered the same structures containing phosphorus, nitrogen, and the Group 16 element. Throughout, we denote the cyclic isomers with a "c" – for example, cyclic PON is denoted cPON. In instances where several elements in the Group 15 or Group 16 series are referenced for comparison, "G15" and "G16", respectively, are used (e.g., P–G16 includes P–O, P–S, P–Se, and P–Te).

Table 3.1 includes the Group 15 and Group 16 congeners considered in the present study and is divided into blocks of isomers [O,P, and N (Block **I**); O, P, and P (Block **II**); etc.]. The isomers within these blocks are arranged in order of increasing relative energy. This energetic order is determined from energy extrapolations to the complete basis set limit of CCSDT(Q) with added Δ_{ZPVE}, Δ_{core}, Δ_{rel}, and Δ_{DBOC} corrections (see Theoretical Methods). Table 3.1 also includes the computed r_e bond lengths and angles for all structures.

3.4.1 A. Block I [O,N,P]

The computed ONP bond lengths nicely agree with the substitution structures (r_s) reported by Okabayashi *et al.*[130] from microwave spectroscopy experiments [1.1950(1) and 1.5165(1) Å versus computed values of 1.191 and 1.526 Å, respectively]. The r_s bond distances often fall between r_0 and r_e bond distances and provide a better approximation to r_e than the vibrationally averaged r_g geometries.[173] Natural Resonance Theory (NRT)[29,164,165] computations predict that the O-N and N-P bonds in ONP resonate between a single and double bond and a double and triple bond, respectively. For OPN, NRT indicates that the O-P and P-N bonds display single-double and double-triple bond resonances, respectively. The P-N double-triple bond resonance is expected, as the computed bond lengths in OPN and ONP lie between

the well-studied[174,175] P-N triple bond (1.491 Å) in PN and the phosphorous-nitrogen double bond length range of 1.50-1.58 Å as outlined by Pohl.[176,177] The cyclic structure (cPON) displays a P-N double bond along with O-P and O-N single bonds, as expected. These bond orders are supported by Wiberg Bond Index[166] (WBI) values of 1.63, 0.92, and 0.93, respectively (see Table 3.2). By constraining the ∠PON bond angle to 180°, we were able to characterize linear PON; both the phosphorus and the nitrogen atoms are double-bonded to oxygen.

The similarity in bonding between OPN and ONP necessitates careful examination of their energy ordering.[37,38] The focal point table for the relative energy extrapolation is shown in Table 3.3. Note that the electronic energies in Table 3.3 display a strong basis set dependence; single-point energy computations with triple-ζ or smaller size basis sets show ONP to be lower in energy than OPN even at the CCSDT(Q) level of theory! OPN is only shown to be lower in energy than ONP once a quadruple-ζ or larger size basis is applied. In total, OPN is found to be 1.91 kcal mol^{-1} lower in energy than ONP, which agrees qualitatively with the excellent recent study of Grant *et al.*[38] The slight disparity between our value and theirs (1.68 kcal mol^{-1}) largely derives from our inclusion of full-triple and perturbative-quadruple excitations, which shifts the extrapolated electronic energy higher by 0.26 kcal mol^{-1}. Our anharmonic Δ_{ZPVE} value of 0.92 kcal mol^{-1} is the largest correction to the energy and agrees well with the 0.91 kcal mol^{-1} value computed by Grant, Dixon, Kemeny, and Francisco.[38]

The focal point result affirms the notions of Zeng, Becker, and Willner,[133] who suggested that the increased electron delocalization induced by positioning the electropositive phosphorus atom between the more electronegative oxygen and nitrogen atoms contributes to OPN being the lowest energy isomer. The cPON isomer is the third highest in energy because of the significant ring strain, which results from the obligatory deviation from ideal bond angles.[178] The structure of linear PON was obtained by constraining the bond angle to 180°.

Unsurprisingly, linear PON is the highest energy Block **I** isomer, and its destabilization with respect to OPN and ONP arises largely from the oxygen atom being in the central position. As the second most electronegative of the elements, oxygen is most stable in situations where it can have localized electron density, e.g., lone electron pairs, in addition to sharing electrons through covalent bonding. However, since PON has only 16 valence electrons, the central oxygen must share all of its valence electrons through covalent bonding with the phosphorus and nitrogen.

The computed anharmonic vibrational frequencies of OPN, SPN, OPP, and their isomers are reported in Table 3.4. For the Block **I** molecules, we compare our results to the argon matrix experiments of Zeng *et al.*[133] Our predicted fundamentals correspond well with theirs, with an average difference of 0.12%. However, our N-O stretch value (1774.4 cm^{-1}) deviates from that of Zeng by roughly 23 cm^{-1} , but is only 17 cm^{-1} from the gas phase values of Bell *et al.*[179,180] The computed normalized anharmonic ONP intensities agree exceptionally well with the normalized intensities from the argon matrices. Computed rotational constants are tabulated on page S2 of the Supporting Information.

3.4.2 B. Blocks II [O,P,P], III[O,P,As], and IV[O,P,Sb]

Much like for OPN, our NRT data show that the phosphorus-centered linear congeners (OPP, OPAs, and OPSb) all display resonance structures: the O-P bonds resonate between a single and double bond, while the P-G15 bonds resonate between a double and triple bond. The G15-centered linear structures display single-double and double-triple bond resonances for O-G15 and P-G15, respectively. As in PON, the linear oxygen-centered Group 15 congeners exhibit double bonding between the oxygen and both the phosphorus and Group 15 element.

For the cyclic structures (cPOP, cPOAs, and cPOSb) the WBI results suggest that the O-P and O-G15 bonds are always single bonds, and the P-G15 bond is consistently a double bond, but the bonding character of the double bond changes as one moves down the Group 15

congeners. The NBO data reveal that the P-N bond in cPON has significant covalent character despite the electronegativity difference between the phosphorus and nitrogen atoms. In the heavier Group 15 congener, cPOP, the P-P double bond becomes entirely covalent since the electronegativities of the two phosphorus atoms are equal. The P-As and P-Sb bonds become less covalent as the Group 15 element becomes more electropositive. WBI data also indicate that the O-G15 bond gets weaker as one moves down the congener series (the O-G15 bond has WBI values of 0.93, 0.79, 0.74, and 0.66 for the congeners involving nitrogen, phosphorus, arsenic, and antimony atoms, respectively). Furthermore, the O-G15 bond gradually decreases in covalent character as one moves down the congener series due to the increasing electronegativity difference between oxygen and the Group 15 element.

Figure 3.1 shows the relative energies of the cyclic and linear phosphorus-, oxygen-, and G15-centered isomers of each Group 15 congener as the congeners increase in atomic mass. Here, the relative energies of the linear phosphorus-, oxygen-, and G15-centered structures are indicated by green circles, purple squares, and blue diamonds, respectively, and the relative energies of the cyclic isomers are indicated with grey triangles. For example, the green circle above [O,P,N] represents the relative energy of OPN to the rest of the Block **I** molecules, while the blue diamond above [O,P,As] represents the relative energy of OAsP with respect to the rest of the Block **III** molecules. As demonstrated in Figure 3.1, the phosphorus-centered structures are consistently the lowest in energy. This is due to their resonance stabilization, which promotes electron delocalization throughout the molecule. The cyclic isomers gradually decrease in energy with respect to the lowest energy isomer as one moves down the congener series. The decrease in covalent bonding character as the congeners become more electronegative frees the molecule from the destabilizing effects of the 3-membered-ring strain. For example, cPON is highly destabilized with respect to the lowest energy isomer, OPN, because the molecule is primarily bound by covalent bonds that cause significant ring strain. However, since the O-G15 bond becomes less covalent for

heavier congeners, the molecule begins to resemble an oxygen atom coordinated to a P-G15 moiety.

As for PON, oxygen-centered and G15-centered linear isomers were computed by constraining the bond angle to 180°. Excluding the Block **IV** antimony congeners, the oxygen-centered isomers are consistently the highest energy Group 15 congeners. This ordering arises from the highly electronegative oxygen being forced to fill its octet by sharing electrons instead of using localized lone electron pairs, yielding an electron deficient oxygen, which destabilizes the molecule and increases its energy. The G15-centered atoms are initially the second lowest energy isomers of each series, as observed with ONP. However, the lower period Group 15 elements have more p- and d- orbitals that exhibit preference for 90° bond angles;[178] hence, constraining the G15-centered molecules to linearity causes angle strain in the molecule. Heavier main group elements also exhibit isovalent hybridization to limit the effect of Pauli repulsion between doubly-occupied 2s atomic orbitals.[181] The result is stronger σ bonds and weaker π bonds. As such, σ-bond energy increments are significantly larger than π-bond energy increments,[181] rendering a preference for bond orders ≤ 1. These destabilizing effects are exemplified in OSbP, which has the highest relative energy of the antimony isomers. The focal point tables for the structures in Blocks **II**, **III**, and **IV** are included the Supporting Information (pp. S4-S7).

Anharmonic vibrational frequencies were computed for the three [O,P,P] isomers. The O-P stretch of OPP is the only frequency of the [O,P,P] isomers to have been experimentally determined. Our result of 1274.6 cm^{-1} agrees within 3 cm^{-1} of Bell's laser spectroscopy value of 1277.6.[182] Additionally, our normalized anharmonic intensites for OPP suggest that the P-O stretch is significantly stronger than the other two modes, with normalized intensities of 100, 3, and 2, respectively. Accordingly, it is not surprising that the other two modes of OPP have not yet been experimentally determined. For the OPP molecule, our B_e and B_0

values of 3870.6774133 MHz and 3862.20897779 MHz are within 1 percent of the experimental microwave spectrocopy results of 3917.9730 MHZ and 3907.6693 MHz.[183]

3.4.3 C. Blocks V [S,N,P], VI [Se,N,P], and VII [Te,N,P]

The phosphorus- and nitrogen-centered isomers of the Group 16 congeners (shown in Blocks **V**-**VII** of Table 1) exhibit resonance structures similar to those of the phosphorus- and G15-centered congeners of the Group 15 series. The NRT data indicate that the phosphorus-centered isomers have single-double and double-triple bond resonances between the P-G16 and P-N bonds, respectively. Likewise, the nitrogen-centered isomers have single-double and double-triple bond resonances between the N-G16 and N-P bonds, respectively. Finally, the G16-centered isomers have double bonds between the Group 16 atom and the nitrogen and phosphorus atoms. The cyclic isomers have a double bond between the nitrogen and phosphorus atoms with each singly bound to the Group 16 atom.

Figure 3.2 shows the relative energies of the cyclic and linear phosphorus-, nitrogen-, and G16-centered isomers of each Group 16 congener as the congeners increase in atomic weight. Here, the relative energies of the linear phosphorus-, nitrogen-, and G16-centered structures are indicated by blue circles, green squares, and purple diamonds, respectively, and the relative energies of the cyclic isomers are indicated with grey triangles. The focal point tables for the structures in Blocks **V**, **VI**, and **VII** are included the Supporting Information (pp. S7-S10). The nitrogen-centered isomer is consistently the lowest-energy isomer of the Group 16 series because its position between the two more electropostive elements fosters electron delocalization throughout the molecule and promotes stabilization. Akin to PON, the G16-centered isomers were computed by constraining the bond angle to 180°. These isomers consistently have the highest relative energies, as was seen in the Group 15 congeners. This again arises from the electronegative Group 16 atom being forced to fill its octet by sharing electrons instead of using localized lone electron pairs, yielding electron deficient Group 16

atoms, which destabilize the molecules and increases the energy. The lower period G16-centered molecules are also destabilized by the same Coulombic repulsion that affected the G15-centered isomers. Further, the high number of p- and d-orbitals in the heavier Group 16 elements prevents their orbitals from hybridizing well with the phosphorus and nitrogen orbitals. As with heavier Group 15 congeners, constraining heavier Group 16 elements to a linear framework induces angle strain as a result of preferred 90° bond angles.

The phosphorus-centered isomers decrease in relative energy for heavier congeners. The primary stabilizing factor for these species is the electron delocalization that arises from the electropositive phosphorus atom being between two more electronegative elements. This arrangement works best for the oxygen congener as oxygen and nitrogen are significantly more electronegative than phosphorus. For the sulfur congener, the phosphorus atom is still the most electropositive element but is similar to sulfur, which causes an increase in its relative energy. However, as one reaches the selenium and tellurium structures, the increasing electropositivity of the Group 16 elements causes the phosphorus-centered isomers to become disfavored. These heavier Group 16 congeners would prefer a positive charge but are forced to possess a negative charge in the phosphorus-centered isomer. This can be observed in SePN and TePN, where selenium and tellurium atoms have Natural Population Analysis charges of -0.22 e and -0.05 e, respectively, serving to lower the relative energy of phosphorus-centered molecules as one moves down the congener series.

Like the cyclic Group 15 congeners, the cyclic Group 16 congeners decrease in relative energy for heavier elements. However, in contrast to the Group 16 isomers, which become more ionic as one moves down the congener series, the cyclic Group 16 congeners maintain covalent bonding. This consistent bonding is due to the similar electronegativities of nitrogen, phosphorus, and the Group 16 molecules. The heavier cyclic structures are energetically favored over the heavier phosphorus-centered structures because the cyclic framework allows the more electronegative Group 16 atoms to be formally assigned a positive charge, as op-

posed to the phosphorus-centered structures where they are forced to be negative. This effect is observed for cPTeN, where the tellurium atom has a 0.15 e charge as opposed to the -0.05 e charge that it has in TePN, stabilizing the cyclic selenium and tellurium isomers with respect to their phosphorus-centered isomers.

Our anharmonic frequencies for SPN, SNP, and cPSN show good agreement with the argon matrix IR results of Zeng *et al.*[134] The largest deviation between our sulfur congener results and theirs arises from the PN stretch in SNP, where our fundamental of 1386.6 cm^{-1}, is about 15 cm^{-1} higher in comparison to the 1374.1 cm^{-1} argon matrix result. The remaining anharmonic frequencies for SPN, SNP, and cPSN generally show a slight underestimation of the frequency but are well within the expected margin of error for argon matrix values.[184] Additionally, our normalized anharmonic intensities of SPN agree qualitatively with the argon matrix values, while our SNP and cPSN intensities show strong agreement with the argon matrix IR intensities. Since the P-N stretching mode of cPSN has a much lower intensity (11) than the two identified modes (100 and 3), it is not surprising that this mode has not yet been experimentally observed.

3.5 Conclusions

An extensive *ab initio* study of OPN and its linear and cyclic Group 15 (OPP, OPAs, and OPSb) and Group 16 (SPN, SePN, TePN) congeners was conducted. The results of our focal point analysis predict that OPN is 2.7 kcal mol^{-1} lower in energy than ONP, an ordering that persists for larger basis sets (quadruple ζ and higher). The opposite ordering predicted by previous studies was likely the result of using too small of a basis to correctly describe the system. All Group 15 centered linear molecules exhibit resonance, with bonds between two Group 15 atoms displaying double-triple bond resonance and bonds between Group 15 and 16 atoms demonstrating single-double bond resonance. The Group 16 centered linear molecules were all double bonded to each of the outer Group 15 elements. The cyclic isomers

all had the two Group 15 elements double bonded to each other and single bonded to the Group 16 element.

The linear phosphorus-centered molecules are consistently the lowest energy isomers of the Group 15 congeners of OPN by at least 6 kcal mol^{-1}, resulting from their resonance stabilization. Likewise, the nitrogen-centered isomers are always the lowest energy isomers of the Group 16 congeners by at least 5 kcal mol^{-1}. This is due to the electron delocalization induced by placing the electronegative nitrogen atom between the more electropositive phosphorus and Group 16 elements. As one moves down the Group 15 and 16 congeners, the cyclic isomers become the second lowest energy isomers. In the cyclic Group 15 isomers this is brought about by decreased covalent bonding character and ring strain. The cyclic Group 16 molecules are stabilized by a partial positive charge on the Group 16 elements. Our anharmonic vibrational frequencies and rotationally corrected vibrational frequencies exhibited good agreement with the few reported experimental values and should aid in future identification of the [O, P, N]; [O, P, P]; and [S, P, N] isomer series in circumstellar media.

3.6 Supporting Information Available

Data for stationary points, including harmonic vibrational frequencies, rotational constants, dipole moments, and table for focal point extrapolations are available in the supplementary data. This information is available free of charge on the ACS Publications website at DO1:10.1021/acs.jpca.5b09936.

3.7 Acknowledgements

This research was supported by the U.S. National Science Foundation, Grant CHE-1361178. W.T. thanks Dr. Justin Turney for helpful discussions.

3.8 Tables

Table 3.1: Relative energies[a] and optimized geometric parameters (r_e)[b] for isomers of Group 15 and 16 congeners.

Block	Structure ABC	ΔE_{0K}	R_{AB}	R_{BC}	R_{AC}	$\angle ABC$
I	OPN	0.00	1.468	1.501		180.0
	ONP	1.87	1.191	1.526		180.0
	cPON	29.79	1.595	1.775	1.586	55.9
	PON[c]	65.79	1.587	1.218		180.0
II	OPP	0.00	1.473	1.897		180.0
	cPOP	9.09	1.742	1.742	1.987	69.5
	POP[c]	39.46	1.591	1.591		180.0
III	OPAs	0.00	1.418	2.001		180.0
	cPOAs	10.72	1.580	1.992	2.128	72.1
	OAsP[c]	31.74	1.563	1.997		180.0
	POAs[c]	40.19	1.577	1.730		180.0
IV	OPSb	0.00	1.430	2.171		180.0
	cPOSb	6.49	1.506	2.344	2.319	70.3
	POSb[c]	32.44	1.489	1.943		180.0
	OSbP[c]	45.10	1.772	2.144		180.0
V	SNP	0.00	1.564	1.528		180.0
	SPN	14.13	1.897	1.503		180.0
	cPSN	18.35	2.077	1.927	1.584	46.4
	PSN[c]	53.77	1.897	1.486		180.0
VI	SeNP	0.00	1.691	1.494		180.0
	cPSeN	9.47	2.229	2.290	1.527	39.5
	SePN	10.15	1.998	1.472		180.0
	PSeN[c]	68.82	2.003	1.633		180.0
VII	TeNP	0.00	2.004	1.450		180.0
	cPTeN	5.75	2.460	2.213	1.507	37.1
	TePN	12.18	2.293	1.445		180.0
	PTeN[c]	80.31	2.154	1.773		180.0

[a] Energies shown in kcal mol^{-1} from computations at CCSDT(Q)/CBS with added ZPVE, core correlation, relativistic, and diagonal Born-Oppenheimer corrections (see Theoretical Methods).

[b] Geometry parameters computed at CCSD(T)/AVQZ with bond lengths given in Angströms and bond angles in degrees.

[c] Computed by constraining the $\angle$ ABC bond angle to 180°.

Table 3.2: Wiberg Bond Indices of the isomers of the Group 15 and Group 16 congeners.

Structure ABC	AB	BC	AC
OPN	1.45	2.46	
ONP	1.53	1.97	
PON	1.04	1.45	
cPON	0.92	0.93	1.63
OPP	1.37	2.54	
POP	0.90	0.90	
cPOP	0.79	0.79	2.04
OPAs	1.36	2.48	
OAsP	1.30	2.46	
POAs	0.95	0.78	
cPOAs	0.91	0.74	1.91
OPSb	1.35	2.36	
OSbP	1.18	2.44	
POSb	0.98	0.64	
cPOSb	0.96	0.66	1.85
SPN	1.68	2.39	
SNP	1.29	1.76	
PSN	1.84	1.92	
cPSN	1.00	0.96	1.81
SePN	1.63	2.38	
SeNP	1.17	1.81	
PSeN	1.81	1.84	
cPSeN	0.99	0.92	1.84
TePN	1.54	2.37	
TeNP	0.99	1.85	
PTeN	1.88	1.78	
cPTeN	0.96	0.83	1.90

Table 3.3: Valence Focal Point Analysis for OPN → ONP[a].

basis set	ΔE_eHF	+δMP2	+δCCSD	+δCCSD(T)	+δCCSDT	+δCCSDT(Q)	NET
AVDZ	-0.56	-8.09	+5.38	-2.37	+0.57	-0.07	[-5.13]
AVTZ	+4.41	-8.55	+5.39	-2.44	+0.55	-0.20	[-0.84]
AVQZ	+4.46	-7.75	+5.65	-2.43	+0.56	[-0.20]	[+0.30]
AV5Z	+4.76	-7.34	+5.65	-2.43	[+0.56]	[-0.20]	[+1.00]
CBS Limit	[+4.97]	[-6.91]	[+5.64]	[-2.43]	[+0.56]	[-0.20]	**[+1.64]**

ΔE_{0K} (final) = ΔE_e[CCSDT(Q)/CBS] + Δ_{core} + Δ_{ZPVE} + Δ_{rel} + Δ_{DBOC}
= 1.64 − 0.43 + 0.87 − 0.22 + 0.00 = **1.87 kcal mol^{-1}**

[a] Energies shown in kcal mol^{-1}. Delta (δ) denotes the change in relative energy (ΔE_e) with respect to the preceding level of theory.

Table 3.4: Anharmonic frequencies (cm^{-1}) and normalized[a] infrared intensities (in parenthesis) for OPN, OPP, SPN, and their isomers computed at the CCSD(T)/ANO2 level of theory.

Molecule	Mode Description	Ar Matrix	Gas-phase	Anharmonic Frequency
OPN	Sym Stretch	1463.4 (22)[b]		1450.0 (89)
	Asym Stretch	1041.7 (100)[b]		1032.3 (100)
	Bend	234.1 (47)[b]		233.2 (51)
ONP	N-O Stretch	1751.9 (100)[b]	1757[c]	1774.4 (100)
	P-N Stretch	866.1 (1)[b]	860[d]	870.8 (1)
	Bend	461.4 (1)[b]		465.1 (1)
PON	O-P Stretch			1398.2 (100)
	N-O Stretch			696.8 (0)
	Bend			365.4 (1)
cPON	N-O Stretch			1087.3 (16)
	P-N Stretch			869.8 (100)
	Bend			361.9 (12)
OPP	P-O Stretch	1277.6 (100)[e]		1274.6 (100)
	P-P Stretch			653.4 (3)
	Bend			206.8 (2)
POP	Sym Stretch			1057.3 (100)
	Asy Stretch			594.4 (0)
	Bend			274.3 (89)
cPOP	Sym Stretch			816.7 (100)
	Asym Stretch			611.6 (42)
	Bend			247.9 (18)
SPN	P-N Stretch	1314.1 (55)[f]		1314.4 (32)
	P-S Stretch	637.1 (100)[f]		635.9 (100)
	Bend	196.8 (24)[f]		198.1 (18)
SNP	P-N Stretch	1374.1 (100)[f]		1389.6 (100)
	N-S Stretch	641.2 (1)[f]		637.6 (2)
	Bend	358.1 (4)[f]		353.7 (3)
PSN	S-P Stretch			1239.4 (100)
	N-S Stretch			609.1 (10)
	Bend			204.8 (0)
cPSN	P-N Stretch			1045.2 (11)
	Sym-ring Stretch	540.0 (34)[f]		540.0 (34)
	Asym-ring Stretch	346.1 (100)[f]		336.0 (100)

[a] The highest intensity of each molecule is normalized to 100 with the remaining modes scaled accordingly.

[b] Reference 133

[c] Reference 179

[d] Reference 180

[e] Reference 182

[f] Reference 134

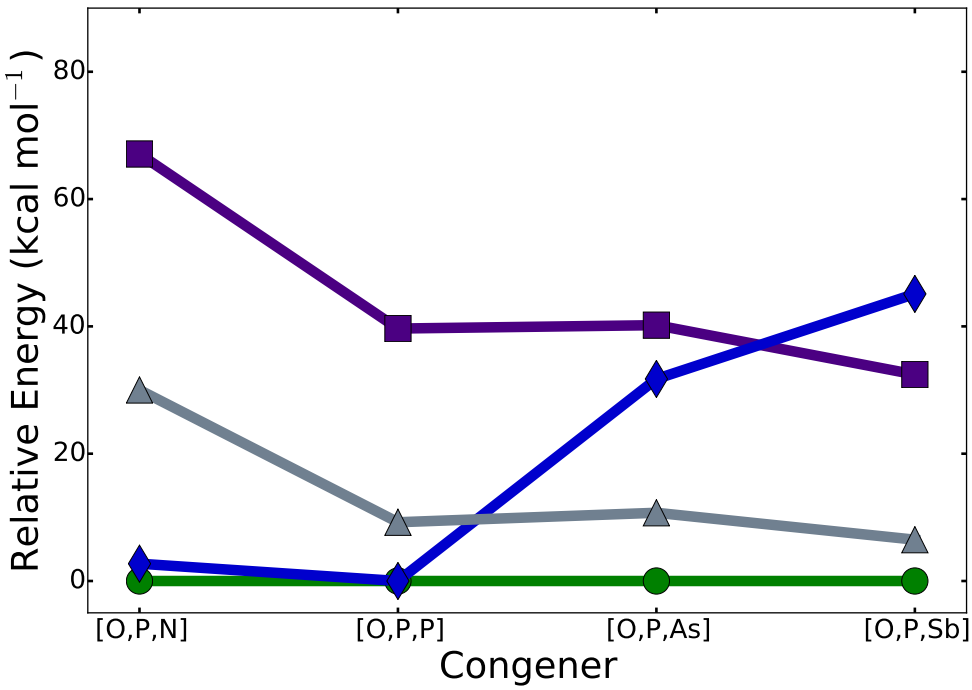

Figure 3.1: ◯ = phosphorus-centered linear structures. ◊ = G15-centered linear structures. □ = oxygen-centered linear structures. △ = cyclic structures. For example, the ◯ above [O,P,N] shows the relative energy of the linear phosphorus-centered isomer OPN.

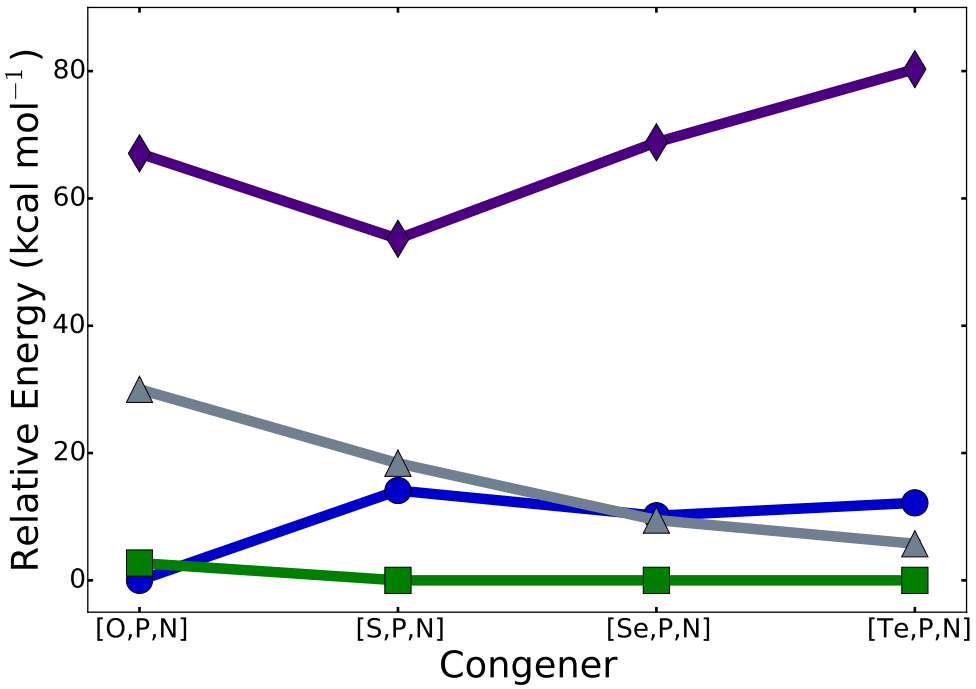

Figure 3.2: ◯ = phosphorus-centered linear structures. ♢ = G16-centered linear structures. □ = nitrogen-centered linear structures. △ = cyclic structures. For example, the ◯ above [O,P,N] shows the relative energy of the linear phosphorus-centered isomer OPN.

Chapter 4

Concluding Remarks

It is clear that high accuracy quantum chemistry has usefulness for both theoreticians and experimentalists. Computational chemists can help settle debates in the chemical literature, assist in the identification of new structures, and explore chemical environments difficult to reproduce in a laboratory setting.

Ab initio quantum chemical methods such as coupled cluster theory have been shown to recover a tremendous amount of electron correlation. These methods may be paired with basis set extrapolation techniques like the focal point approach which take advantage of correlation consistent basis sets in order to extrapolate to the complete basis set limit. When used together, one can produce results with sub kcal mol^{-1} accuracy. Through utilization of second order perturbation theory, computational chemists may compute vibrational data close to cm^{-1} accuracy. Additionally, natural resonance theory can offer insight into the bonding and resonance delocalization of compounds.

The present research computed both r_e and r_g structures for the $^3A_1$ state of C_2H_4 and its isotopologues $^{13}C_2H_4$ and C_2D_4 using CCSD(T)/cc-pVQZ. We also used VPT2 theory to provide the first prediction of ten anharmonic vibrational frequencies of C_2H_4 and its isotopologues. Furthermore, we report rotational constants of the three isotopologues to assist in future identification of twisted triplet ethylene in experimental studies.

A rigorous *ab initio* study of OPN and its Group 15 (OPP, OPAs, and OPSb) and Group 16 (SPN, SePN, TePN) congeners was conducted. Our focal point analysis predicted OPN

to be 1.9 kcal mol^{-1} lower in energy than ONP and that a basis set of at least quadruple zeta size is needed to provide enough flexibility to describe the electron correlation. We utilized natural resonance theory to describe the bonding in all of the studied molecules and identified resonance, when appropriate. We found that the linear phosphorus-centered molecules are consistently the lowest energy isomers of the Group 15 congeners of OPN by at least 6 kcal mol^{-1}, resulting from their resonance stabilization. Likewise, the nitrogen-centered isomers are always the lowest energy isomers of the Group 16 congeners by at least 5 kcal mol^{-1} due to the electron delocalization induced by placing the electronegative nitrogen atom between the more electropositive phosphorus and Group 16 elements. Lastly, we reported anharmonic vibrational frequencies and rotationally corrected vibrational constants of isomers of the potential circumstellar compounds OPN, SPN, and OPP. Our results exhibited good agreement with the few reported experimental values and should aid in their future identification in circumstellar media

Bibliography

[1] Schrödinger, E. *Phys. Rev.* **1926**, *28*, 1049.

[2] Born, M.; Oppenheimer, R. *Ann. Phys.-Berlin* **1927**, *389*, 457.

[3] Hylleras, E. A. *Z. Phys.* **1929**, *54*, 347.

[4] Hylleras, E. A. *Z. Phys.* **1930**, *65*, 209.

[5] Hylleras, E. A. *Adv. Quantum Chem.* **1964**, *1*, 1.

[6] Kutzelnigg, W.; Klopper, W. *J. Chem. Phys.* **1991**, *94*, 1985.

[7] Kutzelnigg, W.; Morgan, J. D. *J. Chem. Phys.* **1992**, *96*, 4484.

[8] Kolos, W.; Wolniewicz, L. *J. Chem. Phys.* **1968**, *49*, 404.

[9] Löwdin, P. O. *Adv. Chem. Phys.* **1959**, *2*, 404.

[10] Roothaan, C. C. J. *Rev. Mod. Phys.* **1951**, *23*, 69.

[11] Saxe, P.; Schaefer, H. F.; Handy, N. C. *Chem. Phys. Lett.* **1981**, *79*, 202.

[12] Slater, J. C. *Phys. Rev.* **1929**, *34*, 1293.

[13] Slater, J. C. *Phys. Rev.* **1930**, *35*, 1930.

[14] Mulliken, R. S. *Phys. Rev.* **1928**, *32*, 168.

[15] Roothan, C. C. J. *Rev. Mod. Phys.* **1960**, *32*, 179.

[16] Ĉížek, J. *J. Chem. Phys.* **1966**, *45*, 4256.

[17] Crawford, T. D.; Schaefer, H. F. *Rev. Comp. Chem.* **2000**, *14*, 33.

[18] Davy, R. D.; Schaefer, H. F. *J. Chem. Phys.* **1982**, *76*, 1910.

[19] Raghavachari, K.; Trucks, G. W.; Pople, J. A.; Head-Gordon, M. *Chem. Phys. Lett.* **1989**, *157*, 479.

[20] Császar, A. G.; Allen, W. D.; Schaefer, H. F. *J. Chem. Phys.* **1998**, *108*, 9751.

[21] East, A. L. L.; Allen, W. D. *J. Chem. Phys.* **1993**, *99*, 4638.

[22] Gonzales, J. M.; Pak, C.; Cox, R. S.; Allen, W. D.; Schaefer, H. F.; Császar, A. G.; Tarczay, G. *Chem. Eur. J.* **2003**, *9*, 2173.

[23] King, R. A.; Allen, W. D.; Schaefer, H. F. *J. Chem. Phys.* **2000**, *112*, 5585.

[24] Karton, A.; Martin, J. M. L. *Theor. Chem. Acc.* **2006**, *115*, 330.

[25] Klopper, W.; Kutzelnigg, W. *J. Mol. Struc.* **1986**, *135*, 339.

[26] Helgaker, T.; Klopper, W.; Koch, H.; Noga, J. *J. Chem. Phys.* **1997**, *106*, 9639.

[27] Pauling, L. *Proc. R. Soc. London* **1993**, *A356*, 433.

[28] Pauling, L.; Wheland, G. W. *J. Chem. Phys.* **1933**, *1*, 362.

[29] Glendening, E. D.; Weinhold, F. *J. Comp. Chem.* **1998**, *19*, 593–609.

[30] Löwdin, P. O. *Phys. Rev.* **1955**, *97*, 1474.

[31] Glendening, E. D.; Reed, A. E.; Carpenter, J. E.; Weinhold, R. *QCPE Bull* **1996**, *10*, 58.

[32] Carpenter, J. E.; Weinhold, F. *J. Mol. Struc Theochem* **1998**, *169*, 41.

[33] Do, T. P. T.; Nixon, K. L.; Fuss, M.; García, G.; Blanco, F.; Brunger, M. J. *J. Chem. Phys.* **2012**, *136*, 184313.

[34] Nguyen, M. T.; Matus, M. H.; William A. Lester, J.; Dixon, D. A. *J. Phys. Chem. A* **2008**, *112*, 2082–2087.

[35] Wu, J.; Schleyer, P. v. R. *Pure Appl. Chem.* **2013**, *85*, 921–940.

[36] Ziurys, L. M.; Milam, S. N.; Apponi, A. J.; Woolf, N. J. *Nature* **2007**, *447*, 1094–1097.

[37] Davy, R. D.; Schaefer, H. F. *J. Chem. Phys.* **1990**, *92*, 5417–5421.

[38] Grant, D. J.; Dixon, D. A.; Kemeny, A. E.; Francisco, J. S. *J. Chem. Phys.* **2008**, *128*, 164305.

[39] Wilkinson, P. G.; Mulliken, R. S. *J. Chem. Phys.* **1955**, *23*, 1895.

[40] Wang, X.; Turner II, W. E.; Agarwal, J.; Schaefer III, H. F. *J. Phys. Chem. A*. **2014**, *118*, 7560–7567.

[41] Aponte, J. C.; Dillon, J. T.; Tarozo, R.; Huang, Y. *J. Chrom. A* **2012**, *1240*, 83–89.

[42] Zechmann, G.; Barbatti, M.; Lischka, H.; Pittner, J.; Bonačić-Koutecký, V. *Chem. Phys. Lett.* **2006**, *418*, 377–382.

[43] Gemein, B.; Peyerimhoff, S. D. *J. Phys. Chem.* **1996**, *100*, 19257–19267.

[44] Barborini, M.; Sorella, S.; Guidoni, L. *J. Chem. Theory Comput.* **2012**, *8*, 1260–1269.

[45] Qi, F.; Sorkhabi, O.; Suits, A. G. *J. Chem. Phys.* **2000**, *112*, 10707–10710.

[46] Clabo, D.; Allen, W.; Remington, R.; Yamaguchi, Y.; Schaefer III, H. *Chem. Phys.* **1988**, *123*, 187–239.

[47] Lee, T. J.; Allen, W. D.; Schaefer III, H. F. *J. Chem. Phys.* **1987**, *87*, 7062.

[48] Murray, C. W.; Handy, N. C.; Amos, R. D. *J. Chem. Phys.* **1993**, *98*, 7145–7151.

[49] Pople, J. A.; Krishnan, R.; Schlegel, H. B.; Binkley, J. S. *Int. J. Quantum Chem.: Symp.* **1979**, *13*, 225–241.

[50] Machida, K.; Tanaka, Y. *J. Chem. Phys.* **1974**, *61*, 5040.

[51] Crawford, B. L.; Lancaster, J. E.; Inskeep, R. *J. Chem. Phys.* **1953**, *21*, 678.

[52] Arnett, R. L.; Crawford, B. L. *J. Chem. Phys.* **1950**, *18*, 118.

[53] Duncan, J. L.; Wright, I. J.; Van Lerberghe, D. *J. Mol. Spectrosc.* **1972**, *42*, 463–477.

[54] Van Lerberghe, D.; Wright, I. J.; Duncan, J. L. *J. Mol. Spectrosc.* **1972**, *42*, 251–273.

[55] Duncan, J. L. *Mol. Phys.* **1974**, *28*, 1177–1191.

[56] Duncan, J. L.; Mills, I. M. *Chem. Phys. Lett.* **1988**, *145*, 347–353.

[57] Duncan, J. L.; McKean, D. C.; Torto, I.; Brown, A.; Ferguson, A. M. *J. Chem. Soc., Faraday Trans. 2* **1988**, *84*, 1423–1442.

[58] Duncan, J. L.; Ferguson, A. M. *J. Chem. Phys.* **1988**, *89*, 4216.

[59] Duncan, J. L.; Robertson, G. E. *J. Mol. Spectrosc.* **1991**, *145*, 251–261.

[60] Duncan, J. L.; Ferguson, A. M.; Goodlad, S. T. *Spectrochimi. Acta A* **1993**, *49*, 149–160.

[61] Duncan, J. L. *Mol. Phys.* **1994**, *83*, 159–169.

[62] Duncan, J. L.; Hamilton, E. *J. Mol. Struct.* **1981**, *76*, 65–80.

[63] Duncan, J. L.; McKean, D. C.; Mallinso, P. D. *J. Mol. Spectrosc.* **1973**, *45*, 221–246.

[64] Van Veen, E. H. *Chem. Phys. Lett.* **1976**, *41*, 540–543.

[65] Sueoka, O.; Mori, S. *J. Phys. Chem. B* **1986**, *19*, 4035–4050.

[66] Szmytkowski, C.; Kwitnewski, S.; Ptasinska-Denga, *Phys. Rev. A* **2003**, *68*, 032715.

[67] Allan, M. *Chem. Phys. Lett.* **1994**, *225*, 156–160.

[68] Allan, M.; Winstead, C.; McKoy, V. B. *Phys. Rev. A* **2008**, *77*, 042715.

[69] Rescigno, T. N.; Schneider, B. I. *Phys. Rev. A* **1992**, *45*, 2894–2902.

[70] Asmis, K. R.; Allan, M. *J. Chem. Phys.* **1997**, *106*, 7044.

[71] Wickramarachchi, P.; Palihawadana, P.; Villela, G.; Ariyasinghe, W. M. *Nucl. Instr. Meth. Phys. Res. Sect. B* **2009**, *267*, 3391–3394.

[72] da Costa, R. F.; Bettega, M. H. F.; Ferreira, L. G.; Lima, M. A. P. *J. Phys.: Conf. Ser.* **2007**, *88*, 012028.

[73] da Costa, R. F.; Bettega, M. H. F.; Lima, M. A. P. *Phys. Rev. A* **2008**, *77*, 042723.

[74] Brongersma, H. H.; Boerboom, A. J. H.; Kistemaker, J. *Physica* **1969**, *44*, 449–472.

[75] Kim, G.-S.; Nguyen, T. L.; Mebel, A. M.; Lin, S. H.; Nguyen, M. T. *J. Phys. Chem. A* **2003**, *107*, 1788–1796.

[76] Mulliken, R. S. *J. Chem. Phys.* **1977**, *66*, 2448–2451.

[77] Mulliken, R. S. *J. Chem. Phys.* **1979**, *71*, 556–557.

[78] Wilden, D. G.; Comer, J. *J. Phys. B: At. Mol. Phys.* **1979**, *12*, L371–L375.

[79] Wilden, D. G.; Comer, J. *J. Phys. Chem. B* **1980**, *13*, 1009–1021.

[80] Raghavachari, K.; Trucks, G. W.; Pople, J. A.; Head-Gordon, M. *Chem. Phys. Lett.* **1989**, *157*, 479–483.

[81] Stanton, J. F. *Chem. Phys. Lett.* **1997**, *281*, 130–134.

[82] Watts, J. D.; Gauss, J.; Bartlett, R. J. *Chem. Phys. Lett.* **1992**, *200*, 1–7.

[83] Watts, J. D.; Gauss, J.; Bartlett, R. J. *J. Chem. Phys.* **1993**, *98*, 8718.

[84] Hampel, C.; Peterson, K. A.; Werner, H.-J. *Chem. Phys. Lett.* **1992**, *190*, 1–12.

[85] Deegan, M. J. O.; Knowles, P. J. *Chem. Phys. Lett.* **1994**, *227*, 321–326.

[86] Dunning, T. H. *J. Chem. Phys.* **1989**, *90*, 1007.

[87] CFOUR, A Quantum Chemical Program Package Written by J.F. Stanton, J. Gauss, J.D. Watts, P.G. Szalay, R.J. Bartlett with contributions from A.A. Auer, D.E. Bernholdt, O.Christiansen, M.E. Harding, M. Heckert, O. Heun, C. Huber, D. Jonsson, J. Jusélius, W.J. Lauderdale, T. Metzroth, C. Michauk, D.P. O'Neill, D.R. Price, K. Ruud, F. Schiffmann, A. Tajti, M.E. Varner, J . Vázquez and the integral packages: Molecule (J. Almlöf and P.R. Taylor), Props (P.R. Taylor), Abacus (T. Helgaker, H.J. Aa. Jensen, P. Jørgensen, and J. Olsen), and ECP routines by A.V. Mitin and C. van Wüllen. For the current version see, http://www.cfour.de.

[88] Stanton, J. *J. Chem. Phys.* **1994**, *101*, 371–374.

[89] Krylov, A. *J. Chem. Phys.* **2000**, *113*, 6052–6062.

[90] Szalay, P. G.; Gauss, J.; Stanton, J. F. *Theor. Chem. Acc.* **1998**, *100*, 5–11.

[91] Harding, M. E.; Metzroth, T.; Gauss, J.; Auer, A. A. *J. Chem. Theory Comput.* **2008**, *4*, 64–74.

[92] Ruden, T. A.; Helgaker, T.; Jøgensen, P.; Olsen, J. *J. Chem. Phys.* **2004**, *121*, 5874–5884.

[93] Koput, J.; Peterson, K. A. *J. Chem. Phys.* **2006**, *125*, 044306.

[94] Rauhut, G.; Knizia, G.; Werner, H.-J. *J. Chem. Phys.* **2009**, *130*, 054105.

[95] Nielsen, H. H. *Rev. Mod. Phys.* **1951**, *23*, 90–136.

[96] Kuchitsu, K. In *Accurate Molecular Structures: Their Determination and Importance*; Domenicano, A., Hargittai, I., Eds.; Oxford University Press, 1992; pp 14–46.

[97] Mills, I. M. *J. Phys. Chem.* **1976**, *80*, 1187–1188.

[98] Gauss, J.; Cremer, D.; Stanton, J. F. *J. Phys. Chem. A* **2000**, *104*, 1319–1324.

[99] Bartell, L. S.; Higginbotham, H. K. *J. Chem. Phys.* **1965**, *42*, 851.

[100] Wu, J. I.; Fernández, I.; Mo, Y.; Schleyer, P. v. R. *J. Chem. Theory Comput.* **2012**, *8*, 1280–1287.

[101] Nielsen, H. H. *Phys. Rev.* **1945**, *68*, 181–191.

[102] Mills, I. M. In *Molecular Spectroscopy: Modern Research*; Rao, K. N., Mathews, C. W., Eds.; Academic Press, 1972; pp 115–140.

[103] Kivelson, D.; E. Bright Wilson, J. *J. Chem. Phys.* **1952**, *20*, 1575–1579.

[104] Plíva, J. *J. Mol. Spectrosc.* **1990**, *139*, 278–285.

[105] Auer, A. A.; Gauss, J. *Phys. Chem. Chem. Phys.* **2001**, *3*, 3001–3005.

[106] Hegelund, F.; Duncan, J. L.; McKean, D. C. *J. Mol. Spectrosc.* **1977**, *65*, 366–378.

[107] Cernicharo, J.; Kahane, C.; Guelin, M.; Hein, H. *Astron. Astrophys.* **1987**, *181*, L9–L12.

[108] Ohishi, M.; Kaifu, N.; Kawaguchi, K.; Murakami, A.; Saito, S.; Yamamoto, S.; Ishikawa, S.; Fujita, Y.; Shiratori, Y.; Irvine, W. M. *Astrophys. J.* **1989**, *345*, L83–L86.

[109] Bell, M. B.; Avery, L. W.; Feldman, P. A. *Astrophys. J.* **1993**, *417*, L37–L40.

[110] Aitken, D. K.; Smith, C. H.; James, S. D.; Roche, P. F.; Hyland, A. R.; McGregor, P. J. *Mon. Not. R. Astron. Soc.* **1988**, *235*, P19–P23.

[111] Rank, D. M.; Pinto, P. A.; Woosley, S. E.; Bregman, J. D.; Witteborn, F. C. *Nature* **1988**, *331*, 505–506.

[112] Rouche, P. F.; Aitken, D. K.; Smith, C. H. *Mon. Not. R. Astron. Soc.* **1993**, *261*, 522–534.

[113] Wooden, D. H.; Rank, D. M.; Bergman, J. D.; Witteborn, F. C.; Tielens, A. G. G. M.; Cohen, M.; Pinto, P. A.; Axelrod, T. S. *Astrophys. J. Suppl. S.* **1993**, *88*, 477–507.

[114] Ziurys, L. M. *Proc. Natl. Acad. Sci. USA* **2006**, *103*, 12274–12279.

[115] Tenenbaum, E. D.; Woolf, N. J.; Ziurys, L. M. *Astrophys. J.* **2007**, *666*, L29–L32.

[116] Ziurys, L. M. *Astrophys. J.* **1987**, *321*, L81–L85.

[117] Guelin, M.; Cernicharo, J.; Paubert, G.; Turner, B. E. *Astron. Astrophys.* **1990**, *230*, L9–L11.

[118] Agundez, M.; Cernicharo, J.; Guelin, M. *Astrophys. J.* **2007**, *662*, L91–L94.

[119] Halfen, D. T.; Clouthier, D. J.; Ziurys, L. M. *Astrophys. J. Lett.* **2008**, *677*, L101–L104.

[120] Milam, S. N.; Halfen, D. T.; Tenenbaum, E. D.; Apponi, A. J.; Woolf, N. J.; Ziurys, L. M. *Astrophys. J.* **2008**, *684*, 618–625.

[121] Tenenbaum, E. D.; Dodd, J. L.; Milam, S. N.; Woolf, N. J.; Ziurys, L. M. *Astrophys. J. Suppl. S.* **2010**, *190*, 348–417.

[122] De Beck, E.; Kaminski, T.; Patel, N. A.; Young, K. H.; Gottlieb, C. A. *Astron. Astrophys.* **2013**, *558*, A132.

[123] Agundez, M.; Cernicharo, J.; Guelin, M. *Astron. Astrophys.* **2014**, *570*, A45.

[124] Ioppolo, S.; Fedoseev, G.; Minissale, M.; Congiu, E.; Dulieu, F.; Linnartz, H. *Phys. Chem. Chem. Phys.* **2014**, *16*, 8270–8282.

[125] Omont, A.; Lucas, R.; Morris, M.; Guilloteau, S. *Astron. Astrophys.* **1993**, *267*, 490–514.

[126] Yildiz, U. A. et al. *Astron. Astrophys.* **2013**, *558*, A58.

[127] Millar, T. J.; Bennett, A.; Herbst, E. *Mon. Not. R. Astron. Soc.* **1987**, *229*, P41–P44.

[128] Bell, I. S.; Hamilton, P. A.; Davies, P. B. *Mol. Phys.* **1988**, *94*, 685–691.

[129] Ahlrichs, R.; Schunck, S.; Schnöckel, H. *Angew. Chem. Int. Ed.* **1988**, *100*, 418–420.

[130] Okabayashi, T.; Yamazaki, E.; Tanimoto, M. *J. Chem. Phys.* **1999**, *111*, 3012–3017.

[131] Tessier, F.; Navrotsky, A. *Chem. Mater.* **2000**, *12*, 148–154.

[132] Peterson, K. A.; Woon, D. E.; Dunning, T. H. *J. Chem. Phys.* **1994**, *100*, 7410–7415.

[133] Zeng, X.; Beckers, H.; Willner, H. *J. Am. Chem. Soc.* **2011**, *133*, 20696–20699.

[134] Zeng, Z.; Beckers, H.; Willner, H.; Francisco, J. S. *Angew. Chem. Int. Ed.* **2012**, *51*, 3334–3339.

[135] Himmel, H.; Linti, G. *Angew. Chem. Int. Ed.* **2012**, *51*, 5541–5542.

[136] Theis, R. A.; Fortenberry, R. C. *J. Phys. Chem. A* **2015**, *119*, 4915–4922.

[137] Fortenberry, R. C.; Lee, T. J. *Mol. Phys.* **2015**, *113*, 2012–2017.

[138] Fortenberry, R. C.; Francisco, J. S. *J. Chem. Phys.* **2015**, *143*, 084308.

[139] Yazidi, O.; Houria, A. B.; Francisco, J. S.; Hochlaf, M. *J. Chem. Phys.* **2013**, *138*, 104318.

[140] Compaan, K. R.; Agarwal, J.; Dye, B.; Yamaguchi, Y.; Schaefer, H. F. *Astrophys. J.* **2013**, *778*, 125.

[141] Cisek, J. *J. Adv. Chem. Phys.* **1969**, *14*, 35–89.

[142] Purvis, G. D.; Bartlett, R. J. *J. Chem. Phys.* **1982**, *76*, 1910–1918.

[143] Scuseria, G. E.; Janssen, C. L.; Schaefer, H. F. *J. Chem. Phys.* **1988**, *89*, 7382–7387.

[144] Pople, J. A.; Head-Gordon, M.; Raghavachari, K. *J. Chem. Phys.* **1987**, *87*, 5968–5975.

[145] Kendall, R. A.; Dunning, T. H.; Harrison, R. J. *J. Chem. Phys.* **1992**, *96*, 6796–6806.

[146] Dunning, T. H.; Peterson, K. A.; Wilson, K. A. *J. Chem. Phys.* **2001**, *114*, 9244–9253.

[147] Martin, J. M. L. *J. Chem. Phys.* **1998**, *108*, 2791–2800.

[148] Martin, J. M. L.; Uzan, O. *Chem. Phys. Lett.* **1998**, *282*, 16–24.

[149] Bauschlicher, C. W.; Ricca, A. *J. Phys. Chem. A* **1998**, *102*, 8044–8050.

[150] Tarczay, G.; Császár, A. G.; Leininger, M. L.; Klopper, W. *Chem. Phys. Lett.* **2000**, *322*, 119–128.

[151] Peterson, K. A. *J. Chem. Phys.* **2003**, *119*, 11099–11112.

[152] Peterson, K. A.; Figgen, D.; Goll, E.; Stoll, H.; Dolg, M. *J. Chem. Phys.* **2003**, *119*, 11113–11123.

[153] Almlof, J.; Taylor, P. R. *J. Chem. Phys.* **1987**, *86*, 4070–4077.

[154] McCaslin, L.; Stanton, J. F. *Mol. Phys.* **2013**, *111*, 1492–1496.

[155] Wladkowski, B. D.; Allen, W. D.; Brauman, J. I. *J. Phys. Chem.* **1994**, *98*, 13532–13540.

[156] Gonzales, J. M.; Pak, C.; Cox, R. S.; Allen, W. D.; Schaefer, H. F.; Császár, A. G. *Chem. Eur. J.* **2003**, *9*, 2173–2192.

[157] Császár, A. G.; Allen, W. D.; Schaefer, H. F. *J. Chem. Phys.* **1998**, *108*, 9751–9764.

[158] Allen, W. D.; East, A. L. L.; Császár, A. G. In *Structures and Conformations of Non-Rigid Molecules*; Laane, J.; Dakkouri, M.; VanderVeken, B.; Oberhammer, H., Eds.; 343-373: Dordrecht, 1993.

[159] East, A. L. L.; Allen, W. D. *J. Chem. Phys.* **1993**, *99*, 4638–4650.

[160] King, R. A.; Allen, W. D.; Schaefer, H. F. *J. Chem. Phys.* **2000**, *112*, 5585–5592.

[161] Peterson, K. A.; Shepler, B. C.; Figgen, D.; Stoll, H. *J. Phys. Chem. A.* **2006**, *110*, 13877–13883.

[162] NBO 6.0. E. D. Glendening, J, K. Badenhoop, A. E. Reed, J. E. Carpenter, J. A. Bohmann, C. M. Morales, C. R. Landis, and F. Weinhold, Theoretical Chemistry Institute, University of Wisconsin, Madison (2013).

[163] Neese, F. *WIREs Comput. Mol. Sci.* **2012**, *2*, 73–78.

[164] Glendening, E. D.; Weinhold, F. *J. Comp. Chem.* **1998**, *19*, 610–627.

[165] Glendening, E. D.; Badenhoop, J. K.; Weinhold, F. *J. Comp. Chem.* **1998**, *19*, 628–646.

[166] Wiberg, K. B. *Tetrahedron* **1968**, *24*, 1083–1096.

[167] Vyboishchikov, S. F. *Int. J. Quant. Chem.* **2008**, *108*, 708–718.

[168] Becke, A. D. *J. Chem. Phys.* **1993**, *98*, 5648–5652.

[169] Lee, C. T.; Yang, W. T.; Parr, R. G. *Phys. Rev. B* **1988**, *37*, 785–789.

[170] Weigend, F.; Ahlrichs, R. *Phys. Chem. Chem. Phys.* **2005**, *7*, 3297–3305.

[171] Kállay, M.; Gauss, J. *J. Chem. Phys.* **2005**, *123*, 214105.

[172] Kállay, M.; Surján, P. *J. Chem. Phys.* **2001**, *115*, 2945–2954.

[173] Haynes, W. M., Ed. *CRC Handbook of Chemistry and Physics, 94th Edition*; CRC Press: Boca Raton, FL, 2013; pp 9–19.

[174] Wyse, F. C.; Manson, E. L.; Gordy, W. *J. Chem. Phys.* **1972**, *57*, 1106–1108.

[175] Raymonda, J.; Klemperer, W. *J. Chem. Phys* **1971**, *55*, 232–233.

[176] Pohl, S. *Angew. Chem., Int. Ed.* **1976**, *15*, 687–688.

[177] Pohl, S. *Chem. Ber.* **1979**, *112*, 3159–3165.

[178] Anslyn, E. V.; Dougherty, D. A. In *Modern Physical Organic Chemistry*; Murdzek, J., Ed.; University Science Books: Sausalito, California, 2006; p 100.

[179] Bell, I. S.; Hamilton, P. A.; Davies, P. B. *Mol. Phys.* **1998**, *94*, 685.

[180] Liu, Y.; Hamilton, P. A.; Davies, P. B. *J. Mol. Spectrosc.* **2002**, *211*, 107–109.

[181] Kutzelnigg, W. *Angew. Chem. Int. Ed.* **1984**, *23*, 272.

[182] Bell, I. S.; Qian, H.; Hamilton, P. A.; Davies, P. B. *J. Chem. Phys.* **1997**, *107*, 8311–8316.

[183] Bailleux, S.; Bogey, M.; Demuynck, C.; Destombes, J.; Yuyan, L.; Császár, A. G. *J. Chem. Phys.* **1997**, *107*, 8317–8326.

[184] Jacox, M. E. *Chem. Soc. Rev.* **2002**, *31*, 108–115.